



Cite this article: Roche J, Royer CA. 2018
Lessons from pressure denaturation of proteins.
J. R. Soc. Interface **15**: 20180244.
<http://dx.doi.org/10.1098/rsif.2018.0244>

Received: 11 April 2018
Accepted: 13 September 2018

Subject Category:

Life Sciences—Chemistry interface

Subject Areas:

biochemistry, biophysics, chemical biology

Keywords:

protein folding, pressure, protein stability

Author for correspondence:

Catherine A. Royer
e-mail: royerc@rpi.edu

Lessons from pressure denaturation of proteins

Julien Roche¹ and Catherine A. Royer²

¹Department of Biochemistry, Biophysics and Molecular Biology Iowa State University, Ames, IA 50011, USA

²Department of Biological Sciences, Rensselaer Polytechnic Institute, Troy, NY 12180, USA

CAR, 0000-0002-2670-3391

Although it is now relatively well understood how sequence defines and impacts global protein stability in specific structural contexts, the question of how sequence modulates the configurational landscape of proteins remains to be defined. Protein configurational equilibria are generally characterized by using various chemical denaturants or by changing temperature or pH. Another thermodynamic parameter which is less often used in such studies is high hydrostatic pressure. This review discusses the basis for pressure effects on protein structure and stability, and describes how the unique mechanisms of pressure-induced unfolding can provide unique insights into protein conformational landscapes.

1. Introduction

In recent years, advances in experimental and computational methods for the investigation of protein folding, including single molecule methods, ultra-fast perturbation and detection approaches, individual residue observation and improvements in all atom and coarse-grained simulation methods, have greatly expanded and deepened our understanding of protein folding mechanisms and the effects of environmental factors on folding landscapes. Of particular interest in the field is how folding landscapes have been shaped by evolution. Beyond global stability and native state structure, sequences must be optimized for all aspects of protein homeostasis such as turnover, dynamics, conformational heterogeneity and higher-order interactions, all of which impact protein function. Insight into how sequence alters folding landscapes, and not simply the folded state stability, will contribute to understanding how life has evolved to thrive in extreme environments on Earth, and perhaps elsewhere. Such insight would also be of great practical use in the design or modification of proteins for biotechnological or biopharmaceutical applications.

Two current, and not necessarily contradictory, points of view concern the nature of folding landscapes. On the one hand, it is postulated that these landscapes are rather simple, with well-defined folding pathways based on the stability of intrinsic structural units, or foldons [1–3]. On the other hand, many studies have revealed that protein folding landscapes can be rich and complex ([4] and references therein). Both of these points of view were derived from the advanced approaches noted above. While seemingly in opposition, these two viewpoints may be reconciled, as observed folding mechanisms are likely to depend upon a number of factors. These include the exact sequence of the protein under investigation, the observables employed to monitor its behaviour and the method employed to perturb the folded structure. As concerns perturbation methods, most protein folding studies have relied on chemical denaturants, although temperature and force [5] are also used. Another thermodynamic variable, not widely employed, yet that also leads to the unfolding of proteins, is high hydrostatic pressure. This review explores the unique consequences of pressure on protein stability and the unique insights into folding landscapes that pressure can provide.

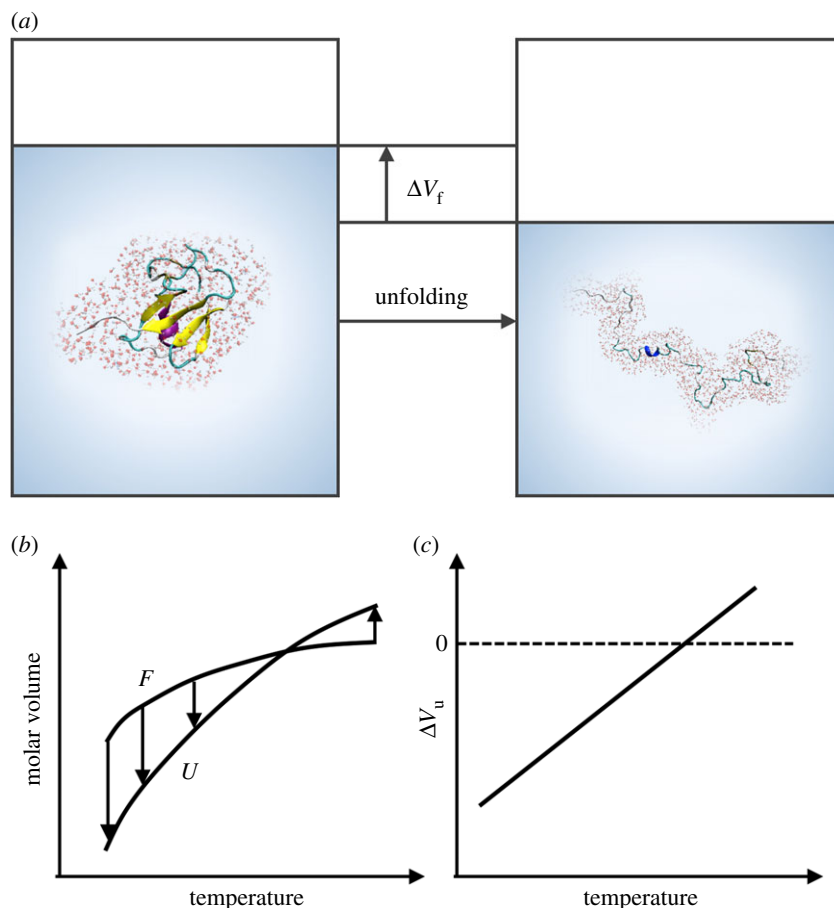


Figure 1. Protein volumetric properties. (a) Schematic depicting the fact that the volume of a molar solution of folded protein is larger than that of a solution of unfolded protein. This is the case at atmospheric pressure. (b) Schematic of the temperature dependence of the volume of a protein folded state and unfolded state. Arrows depict the difference between the two as the volume of the folded state minus the volume of the unfolded state. (c) Schematic of how the difference in volume between the folded and unfolded states of a protein, ΔV_u , changes with temperature. (Online version in colour.)

2. Mechanism of pressure denaturation of proteins

Over 100 years ago in 1914, Percy Bridgman, recipient of the 1946 Nobel Prize in Physics for his high-pressure (HP) work, published a short article in the *Journal of Biological Chemistry* in which he reported that the application of pressure resulted in the coagulation of albumin from egg white [6].

If the white of an egg is subjected to hydrostatic pressure at room temperature, it becomes coagulated, presenting an appearance much like that of a hard boiled egg. ...At room temperature (20 degrees) the limits of pressure necessary to produce the coagulation were fairly well marked. A pressure of 5000 atmospheres (75 000 pounds per square inch) applied for thirty minutes produced a perceptible stiffening of the white, but little more; 6000 atmospheres for thirty minutes produced a coagulation in appearance like curdled milk; while 7000 for thirty minutes resulted in apparently complete coagulation, the white being capable of standing under its own weight.

Over the next century, particularly beginning after World War II, several groups investigated pressure-induced unfolding of monomeric proteins or dissociation of protein oligomers ([7,8] and references therein), yet the mechanism by which pressure leads to protein denaturation remained hotly debated.

Obviously, if pressure results in the unfolding of proteins, the molar volume of the unfolded state must be smaller than that of the folded state (figure 1a). This difference in molar volume is referred to as ΔV_u , the volume change of

unfolding. This quantity is generally rather independent of the pressure at which the protein unfolds. Indeed, volume changes of unfolding extracted from HP spectroscopic studies, typically carried out in the 1000–5000 bar pressure range, have been found to be compatible with those obtained from pressure perturbation calorimetry (PPC), in which a pressure of only five bar (approx. five atmosphere) is used [9–11]. The fact that ΔV_u is pressure independent indicates that the difference in compressibility between the folded state and the unfolded state is negligible. It also means that the effects of pressure on the solvent (water), at least at pressures below 5000 bar, do not contribute significantly to the phenomenon, as these effects would necessarily be pressure-dependent. Simply stated, the volume difference between folded states of proteins and unfolded (and other) states exists at atmospheric pressure. According to Le Chatelier's principle, pressure shifts the equilibrium toward the state(s) that occupies the smallest volume so as to minimize the perturbation.

The question then becomes, why is the molar volume of the unfolded state smaller than that of the folded state? To address this question, one must consider what makes up the molar volume of proteins in aqueous solution, and secondly what may change between the folded and unfolded states. Protein molar volume is made up of the van der Waals volume of the protein atoms, which is invariant with the conformational state of the protein, and the volume of the interacting water molecules. More solvent molecules

interact with the increased accessible surface area (ASA) of the protein exposed upon unfolding, ΔASA . If the density of the interacting solvent molecules is different from that of bulk molecules, this could contribute to the difference in molar volume between the folded and unfolded states. The sign and magnitude of this effect for the hydration of polar and apolar protein surfaces remains under debate. PPC measurements suggest that solvation of polar surfaces may increase solvent density (decrease volume) relative to the bulk, whereas solvation of apolar surfaces may result in a decrease in density (increase in volume) [12,13]. These effects appear to be largest at low temperature, and being of opposite sign, may largely cancel out. Alternatively, it has been proposed based on gas- to liquid-phase transfer and computational studies on protein solvation that both apolar and polar solvation leads to an increase in volume [14–16].

Finally, folded proteins are very well packed [17]. However, they are not perfectly packed. There exist within folded protein structures, small packing defects of varying sizes and shapes [18], which are often devoid of solvent [19,20]. Upon unfolding, these solvent excluded voids are largely eliminated, necessarily decreasing the molar volume. The magnitude of this effect is difficult to ascertain, as determination of cavity volume generally relies on the use of a probe of a particular size to evaluate protein interior voids. Typical software packages recommend the use of a probe with a 1.4 Å radius (i.e. a water molecule; see the discussion in [14]). However, internal void volumes usually do not exhibit the size or shape required to accommodate a water molecule, and hence calculations based on this approach reveal only the largest internal cavities. Makhatadze and co-workers, using a probe size of 0.04 Å, estimated the decrease in void volume between the folded and unfolded states of proteins to be quite large. Moreover, they posit that this large decrease in volume is largely offset by the increased hydration volume, leading to a small decrease (approx. 7%) in total molar volume upon unfolding [16]. Whether polar and apolar hydration contributions offset each other, or whether large contributions from hydration offset an even larger negative contribution from elimination of void volume as suggested by Chen & Makhatadze [14,16], the result is that elimination of internal solvent excluded void volume represents the only major factor favouring pressure-induced unfolding. Indeed, it has been demonstrated that changing the amount of void volume in a protein significantly changes the ΔV_u value [21,22], while changing the size of a protein, which changes the ΔASA , does not [23]. Thus, while a number of theoretical studies provide evidence for differences in density between bulk water and water at protein surfaces [24–26], the fact that experimentally, the volume change of unfolding is not correlated with protein size, and thus the amount of exposed surface area demonstrates that these density differences do not contribute significantly to pressure denaturation of proteins.

3. Protein stability in the P-T plane

The volume changes of unfolding of proteins have generally been found to be negative, i.e. pressure will favour the unfolded state [8]. However, the observation that the ΔV_u could take on positive values, particularly at high temperature [27,28], greatly confused the interpretation of volume

changes associated with protein folding. Indeed, ΔV_u is strongly dependent on temperature, increasing as temperature increases and eventually becoming positive. This and the large increase in heat capacity upon unfolding, ΔC_p , leads to the well-known elliptical phase diagram for protein stability in the P-T plane [27–29]. Most HP unfolding experiments had been performed around room temperature where proteins generally populate the folded state, which explains the preponderance of negative values for ΔV_u found in the literature [8]. The temperature-dependent decrease in the magnitude of ΔV_u arises because the thermal expansivity of the unfolded states of proteins is generally larger than that of folded states (figure 1*b,c*). This difference in thermal expansivity, $\Delta\alpha_u$, can be ascribed, at least in part, to the greater degree of hydration of unfolded proteins, and supports Makhatadze's model in which the hydration contribution to volume changes is always positive [15]. However, the energetic constraints of folded protein structures also limit their thermal expansion, likewise contributing to the amplitude of $\Delta\alpha_u$ [30,31]. Interestingly, a correlation was observed between the number of strong hydrogen bonds, determined by the temperature-dependence chemical shifts of the backbone amide NMR resonances for of a series of cavity containing variants of a hyperstable mutant ($\Delta + \text{PHS}$) of staphylococcal nuclease (Snase) and the thermal expansivity of their folded states [31].

4. On the importance of observables

Key to capturing the complexity of protein folding landscapes is the use of multiple observable parameters to monitor different and complementary aspects of protein structure. The challenge over the years, now largely met, has been to adapt state-of-the-art biophysical instrumentation for use at high hydrostatic pressure. Below are presented a number of techniques for which HP instrumentation is available. For many years, HP biophysics was a tinkerer's (and plumber's) world. However, today commercial HP cells and generating systems are available or are coming online for most of the techniques highlighted below. Progress can yet be made in extending the pressure ranges of the HP cells used, but HP biophysical measurements are now largely routine.

Circular dichroism (CD) and tryptophan fluorescence are among the most commonly used techniques. The former is based on differential absorption of left- and right-handed circularly polarized UV-Vis light. CD measurements in the range of 180–230 nm correspond to absorption by peptide bonds and provide a measure of global backbone secondary structural content. At higher wavelengths near UV, CD can provide information about changes in the tertiary packing of aromatic residues. Infrared absorption in the range of peptide bond vibrational frequencies is another spectroscopic approach that can inform on protein secondary structural content. While CD presents very characteristic signals for α -helix, IR absorption shows very clear peaks for β -structure, although both types of secondary structure, and lack thereof, can be discerned with both techniques. Both CD and IR (usually Fourier transform or FTIR) are composite variables, in that they are the result of the contributions from all peptide bonds in the protein. In terms of their application to HP, for many years only HP FTIR [32], based on the use of diamond anvil cells, was more practical due to birefringence issues in

CD. However, recently a HP CD sample holder was developed based on MgF₂ windows [33]. Also routinely used for many years in HP studies on proteins is UV–Vis absorption of aromatic residues [27,28,34]. UV–Vis absorption spectroscopy provides another composite parameter to describe changes in protein tertiary structure.

Tryptophan fluorescence is in principle, a local probe, although for proteins that contain more than one tryptophan residue, the composite fluorescence signal will contain information concerning the regions around all tryptophan residues in the protein. Tryptophan intensity generally changes upon unfolding (most often it is quenched, but not always) [35]. In addition, tryptophan residues are often found either partially or completely buried in the hydrophobic interior of proteins, in which case their emission will shift red upon unfolding due to solvent relaxation. Note that the relative individual contributions of different tryptophan residues to the overall fluorescence signal depend on their quantum yields and the changes therein upon unfolding [36]. It should be noted as well that tryptophan fluorescence properties are exquisitely sensitive to the polarity and hydration of the environment, such that even distant structural perturbations can have local consequences that are detected via tryptophan fluorescence. HP fluorescence studies of protein folding and interactions have been carried out for over 50 years [37], and commercial instrumentation is available (ISS, Inc. Campaign, IL). HP phosphorescence of proteins has been used to derive pressure-dependent dynamic information [38].

Forster resonance energy transfer (FRET), another fluorescence approach, has also often been used to study protein folding. FRET yields distances and changes therein in the range of 10–100 Å, depending on the dyes used. One HP bulk FRET study concerning the coupled dissociation/unfolding of triose phosphate isomerase has been published [39]. Another study based on triplet–triplet energy transfer revealed a lower volume unlocked state intermediate of the model protein, tendamistat [40]. Most recent studies using FRET to monitor biomolecular conformational transitions involves single molecule (sm)FRET. To our knowledge, there are only two published studies to date of biomolecular folding based on smFRET under HP, one HP smFRET study on DNA hairpin formation [41] and the other on protein folding, both using a capillary system similar to that previously described for use in HP fluorescence correlation measurements [42]. Progress can still be made in rendering the HP capillary system more reliable and easier to use. Nonetheless, we expect that more and more HP single molecule fluorescence studies smFRET, FCS, Number and Brightness, etc. both *in vitro* and *in vivo* will be carried out in the near future.

Small angle X-ray scattering (SAXS) is a low-resolution structural technique applied on biomolecular (and other) solutions. From the scattering intensity profiles as a function of momentum transfer (scattering angle) the molecular size and shape of biomolecules can be inferred. Globular proteins, which exhibit roughly spherical shapes in their folded state, populate more or less extended conformations in their unfolded states, depending upon their sequence and conditions [43,44]. HP synchrotron-based SAXS studies have been used to determine the radius of gyration of pressure-unfolded states of proteins [45–49].

Nuclear magnetic resonance (NMR) provides a host of observables that report on protein structure and dynamics. It was recognized nearly 50 years ago, that if appropriate

instrumentation could be developed, HP NMR could yield a wealth of information about pressure effects on protein structure, stability and dynamics [50–58]. For a review of HP protein NMR, see [59,60] and references therein. The recent design of ceramic HP NMR cells [61–63] and their commercialization (Daedalus, Inc) has expanded the use of HP NMR [22,64–67], which is now routine. Virtually any modern multi-dimensional NMR experiment can now be routinely performed under pressure. HP EPR has also been developed and applied to the study of proteins [68].

5. Unique mechanisms of pressure perturbation versus chemical denaturation

It is now clearly established that the main contributing factor to the decrease in volume between the folded and unfolded states of proteins is the existence in folded protein structures of solvent excluded void volumes that are eliminated upon unfolding. Hence pressure effects on any given protein are due to very specific characteristics of its folded state, i.e. its internal packing density and pattern. This is in contrast to the efficacy of chemical denaturation, the so-called *m-value* = $d\Delta G_w/d[\text{denaturant}]$, as well as the second-order term in the temperature dependence of protein stability, the heat capacity change, ΔC_p , both of which are determined by the ΔASA , an unfolded state property and simply a function of the size of the protein [69]. Moreover, because void volumes are non-uniformly distributed throughout folded protein structures, protein homologues of the same size and structure can have very different volumetric properties, and hence sensitivity to pressure perturbation, while their folding *m-values* in chemical denaturation will be the same, provided their folding is two-state.

To be sure, the underlying energetic architecture of the protein will strongly influence its response to any denaturing perturbation. However, the consequence of the distinct mechanisms for pressure-induced unfolding as opposed to denaturant-induced unfolding is that pressure, based on local properties of the folded state, will not necessarily lead to the same unfolding behaviour as urea, based on a global property of the unfolded state. For example, the degree of population of intermediates, the structural, energetic and dynamic properties of the unfolded state ensemble, and conceivably even the folding pathway(s) can differ between pressure and chemical denaturation. We do not suggest that these differences between denaturing mechanisms and outcomes make pressure a better method than chemical perturbation for studying protein folding. Nor is it any worse. It is simply different. As such, comparison of the results of pressure denaturation with those obtained using chemical denaturants (as well as heat and cold, acid and force) allow a more complete exploration of protein folding landscapes. As is often the case, the results obtained using multiple approaches generally reveal more complexity in any system, than observed if a single approach is used.

6. Model systems for understanding and exploiting high-pressure effects on proteins

Snase has served for many years as a model system for understanding pressure effects on protein folding. One

distinct advantage of Snase for HP unfolding experiments was the fact that it could be purified in very large quantities, and that because of its electrostatic characteristics, could be studied at relatively high concentrations without suffering from aggregation. Moreover, the unfolding of Snase and a large number of mutants by pH, denaturant and temperature was well established (e.g. [70–74]). A large number of structures of Snase were available [75–77], too many at present to enumerate (figure 2a).

We have also used repeat proteins as model systems for understanding pressure effects on proteins, as well as for exploring protein folding landscapes using pressure perturbation. Thanks to their linear architecture, devoid of sequence distant contacts, these proteins are well-suited for testing the effects of size on volumetric properties, as the number of repeats can be manipulated. The linear nature of their folds also provides a simplified backdrop for interpreting the relationships between local and global stability and folding cooperativity. For the two protein systems we have studied, the Ankyrin repeat domain of the Notch protein (Nank) (figure 2b) and the leucine-rich repeat domain of the Anp32 protein (pp32) (figure 2c), an extremely solid characterization of their unfolding by chemical denaturants had been established prior to the pressure studies [82–85].

Using the model systems referenced above, we have examined the effects of amino acid substitution on pressure effects *per se*, and on the folding landscape of the model systems in particular. In addition to the Markley group in Wisconsin, these projects have been carried out in collaboration with Roland Winter in Germany, Bertrand Garcia-Moreno and Doug Barrick at Johns Hopkins, Christian Roumestand in Montpellier and Kazuyuki Akasaka in Japan. What follows is a summary of the lessons learned from these studies.

The first published work concerning the pressure-induced denaturation of Snase, H124L, was carried out in collaboration with the Markley group in Wisconsin. We found that the protein was reversibly denatured by pressure, with a substantial volume change, $\Delta V_u \sim 85 \text{ ml mol}^{-1}$. This led us to investigate a series of variants with mutations that altered the conformational equilibria of the protein. We found that proline to glycine substitutions damped the dynamics of the protein (as ascertained from time resolved fluorescence anisotropy of the single tryptophan residue) and also led to a much smaller ΔV_u value than for the parent H124 L variant [52]. We proposed that the better packing resulting from eliminating cis–trans proline isomerization reactions was responsible for both the damped dynamics and the smaller volume change, although at the time the basis for the volume change had not been demonstrated.

7. What is responsible for the volume change of unfolding of proteins?

Central to the ability to ascertain the factors contributing to the sign and magnitude of ΔV_u is the accuracy with which it can be measured. In particular, using the approaches outlined above, ΔV_u is calculated as the derivative of the free energy change of unfolding, ΔG_u , with respect to pressure. Pressure-induced unfolding profiles from any observable are fit to a two-state model in which $\Delta G_u(p)$ at any pressure is obtained from the expression relating the equilibrium constant for unfolding, K_u , to the value of the observable

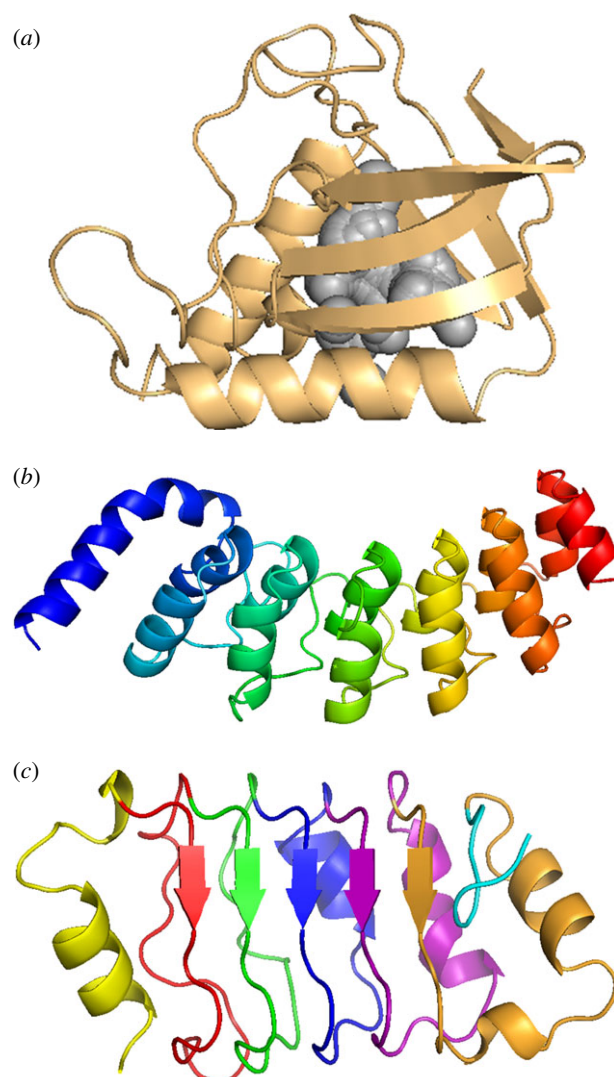


Figure 2. Model protein systems. (a) Staphylococcal nuclease [76]. The grey spheres represent the internal void volume detected using Hollow and a 1.1 Å probe [78]. (b) The ankyrin repeat domain of the Notch receptor (Nank) [79]. Each ankyrin repeat is coloured a different colour in rainbow order from N- to C-terminus. (c) The leucine-rich repeat domain of the Anp32 tumour suppressor protein (pp32) [80]. The N-terminal capping motif is coloured yellow, the C-terminal capping motif is coloured cyan, and repeats 1–5 are coloured red, green, blue, purple and orange, respectively. All protein structures were rendered using PyMol [81]. (Online version in colour.)

parameter at pressure, $O(p)$ and its values for the fully folded and fully unfolded states, O_f and O_u , respectively.

$$\Delta G_u(p) = \Delta G_u(\text{atm}) + p\Delta V_u, \quad (7.1)$$

$$\Delta G_u(p) = -RT \ln K_u(p) \quad (7.2)$$

and

$$K_u(p) = \frac{[U]}{[F]} = \frac{O_f - O(p)}{O(p) - O_u}. \quad (7.3)$$

The value for ΔV_u obtained from fits of the observable to the above equations as a function of pressure will only represent a good approximation of the true value if the transition is a two-state transition. Hence, any study to examine how mutations or changing conditions would modulate the value of ΔV_u must be supported by evidence that the unfolding of our model systems conformed to a two-state transition. One of the best ways to test the two-state hypothesis is to monitor several observables that report on distinct structural parameters. For example, as noted above,

tryptophan fluorescence monitors local tertiary packing, FTIR and CD report on secondary structural content and SAXS reveals the degree of collapse of the protein. Results from a series of pressure-induced unfolding experiments on WT Snase, comparing fluorescence, FTIR and SAXS profiles in collaboration with Roland Winter's group [45,86] supported the notion that pressure-induced unfolding of WT Snase adhered reasonably well to a two-state model. This conclusion was later further supported by results from *HP* multi-dimensional NMR [87].

Direct measurement of the volumetric properties of Snase using pressure and temperature-dependent densitometry, also in collaboration with the Winter group, provided the first straightforward evidence for the relative roles of thermal expansion and isothermal compressibility in defining Snase stability in the P-T plane [11]. The results were in excellent agreement with those extracted from fitting of profiles obtained from SAXS, fluorescence and FTIR, thus corroborating the two-state assumption. Importantly, they showed clearly that the intrinsic differences in volume and the differences in thermal expansion between folded and unfolded states define the ΔV_u value of Snase, as opposed to negligible contributions from differences in compressibility. These results provided the experimental evidence that eventually, along with values of ΔV_u from PPC measurements, allowed construction of an experimental volume diagram for Snase such as that shown in figure 1*b,c* [13]. This ensemble of results on WT Snase underscored the validity of the assumption of two-state unfolding, and the values obtained for the ΔV_u laying the groundwork for investigating the relative importance of cavities and hydration changes.

The first attempt to correlate the contributions of cavities and ΔASA with the value of ΔV_u were carried out using two series of Snase variants. The first set of variants studied were Snase mutants with either cavity-creating or cavity filling substitutions at position 66. WT Snase bears a valine at this position and this residue defines part of the surface of an internal cavity in Snase (figure 2*a*). We carried out tryptophan-detected pressure-induced unfolding of WT Snase and the Snase V66G, V66A and V66 L variants [88]. This latter mutation should act to partially fill the internal cavity present in WT Snase. Based on coordinates kindly provided by the Lattman group (Ed Lattman, 1993, unpublished data), the WT Snase and V66G structures superimposed with an RMSD of only 0.776 Å with only minor readjustments of the side chains around residue 66. Thus, this mutation was expected to create a cavity. We found larger absolute values of ΔV_u for all three mutants. Those for the V66G and V66A mutants were in very good agreement with predictions, while that of the V66 L mutant, while expected to be smaller was slightly larger.

Because the crystal structures for all three variants were not available, the conclusions from this study remained tentative for many years. Then recently, in collaboration with the groups of Bertrand Garcia-Moreno and Christian Roumestand, we measured the volume changes for unfolding of several variants of Snase with alanine substitutions at several different positions [22]. The crystal structures were determined for all variants and revealed cavity creation by these mutations (figure 3*a*). All of the variants, without exception, showed larger absolute values for ΔV_u , as expected (figure 3*b*). One isoleucine to alanine substitution at position 92, opposite the V66 position, resulted in a doubling of the volume change. Further studies with double and triple cavity creating

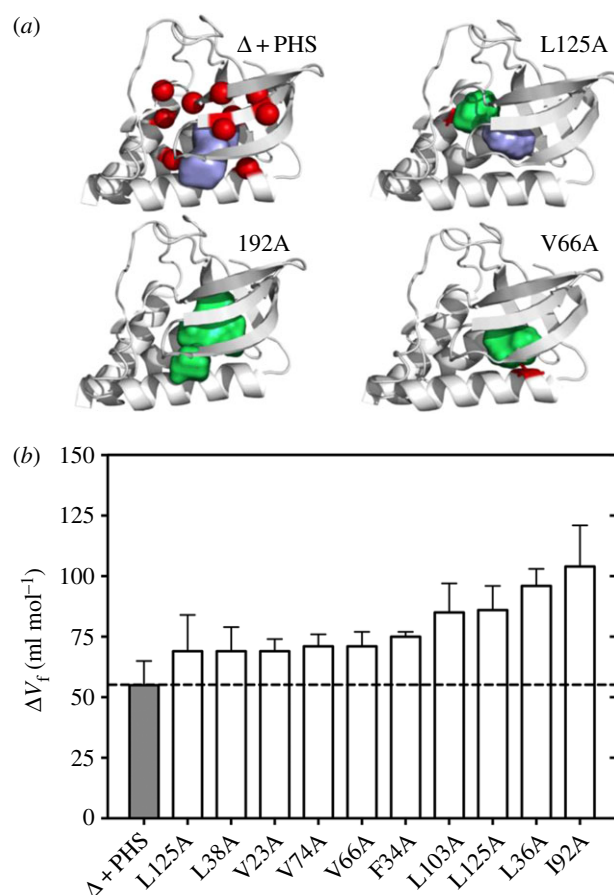


Figure 3. Effects of cavity-creating mutations on the volume change of unfolding of the hystable Snase variant, $\Delta + PHS$. (a) Cartoons of the structures of the Snase $\Delta + PHS$ background, and the L125A, I92A and V66A variants, as indicated [22]. The cavities in purple and green were calculated using McVol [89] and a 1.1 Å probe as described in [22]. (b) Volume change of folding, ΔV_f , for the $\Delta + PHS$ background and 10 variants studied using HP fluorescence. Results first reported in [22]. Error bars represent uncertainty in the value of obtained from rigorous confidence limit testing analysis of three curves at different denaturant concentration for each variant. (Online version in colour.)

mutations revealed a roughly linear relationship between the size of the cavity as assessed from its crystal structure and the magnitude of ΔV_u [90]. Together, and along with work from the Gruner group at Cornell on T4 lysozyme cavity containing variants [21], these studies demonstrated that single amino acid cavity-creating substitutions substantially increase the value of ΔV_u and clearly demonstrate that solvent-excluded voids in the interior of protein structures contribute significantly to pressure-induced protein unfolding.

The second set of variants we interrogated were the so-called m-value mutants of David Shortle. They were chosen because Shortle had proposed that their lower m-values for denaturant unfolding were due to a smaller ΔASA upon unfolding, presumably correlating with residual structure in the unfolded state [91]. The two variants exhibiting the largest and smallest m-values were examined, but no significant difference in the value of ΔV_u was observed, suggesting that differential density of hydrating solvent molecules compared to bulk, and the increase in hydration upon unfolding did not contribute significantly to the value of ΔV_u [92]. However, much later, evidence for deviation from two-state behaviour for at least some of the m-value variants put into question the premise for our experiments to characterize the contribution of ΔASA to ΔV_u .

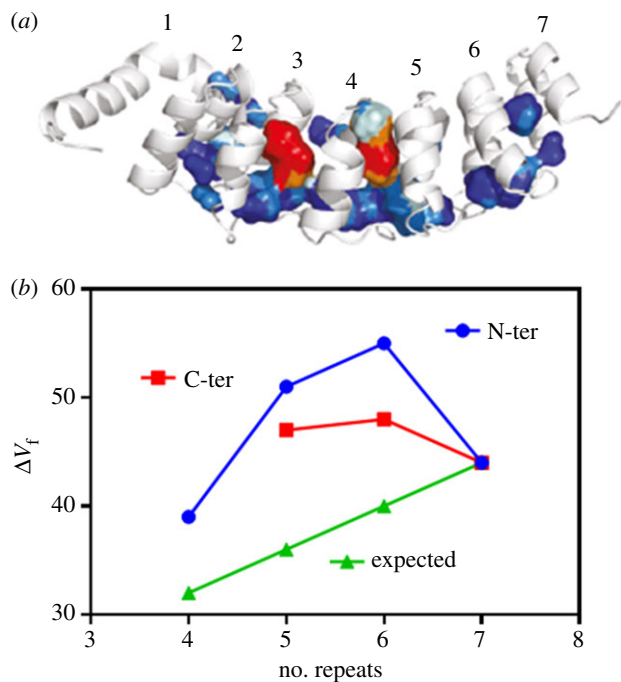


Figure 4. Effect of size on the volume change of unfolding. (a) Cartoon representation of the Nank protein obtained from molecular dynamics simulations showing the internal cavities in red and blue. Red regions are those for which the distance to the closest water molecule is greater than 5 Å, while in blue are those for which water molecules were present at a distance of less than 5 Å as described in [95]. Repeats are numbered 1–7. (b) The dependence of volume change of folding, ΔV_f , determined from HP fluorescence on the size of the protein. In blue are results from variants deleted for 1, 2 and 3 repeats from the N-terminus, and in red are the results from variants deleted for 1 or 2 repeats from the C-terminus. In green is the result that was expected if hydration of exposed surface area and differences in density between bulk and hydrating water molecules were responsible for the value of ΔV_f . Results were first reported in [95]. (Online version in colour.)

We therefore sought a better model system to test the contribution of ΔASA to ΔV_u . The unfolding properties of the Ankyrin repeat domain of the Notch receptor, Nank (figure 2b) and a series of variants deleted for up to three repeats from either the N- or the C-terminus had been characterized in depth by the Barrick group [93]. Their unfolding was cooperative and the energetics additive in terms of repeat and interfacial stability. In collaboration with the Barrick group, we measured the pressure-induced unfolding of the WT full-length Nank with seven repeats, as well as that of Nank 1–6, 1–5, 2–7, 3–7 and 4–7 [23,94]. We found the value of ΔV_u to be totally uncorrelated with the size of the protein (figure 4b). Indeed, deletion of one repeat from either terminus resulted in an increase in the magnitude of ΔV_u . Rather we found that the determinants for the value of ΔV_u to be located in the centre of the protein, where the largest and most hydrophobic cavities are found (figure 4a). These results reinforced our earlier conclusions, that the value of ΔV_u has little or no contribution from changes in density of the solvent molecules interacting with increased exposed surface area in the unfolded versus the folded state.

Figure 5a shows the correlation coefficients between various structural properties of a series of globular proteins and their published ΔV_u values, all measured by high-pressure fluorescence, all at similar temperatures. This plot indicates that the value of ΔV_u is strongly correlated with

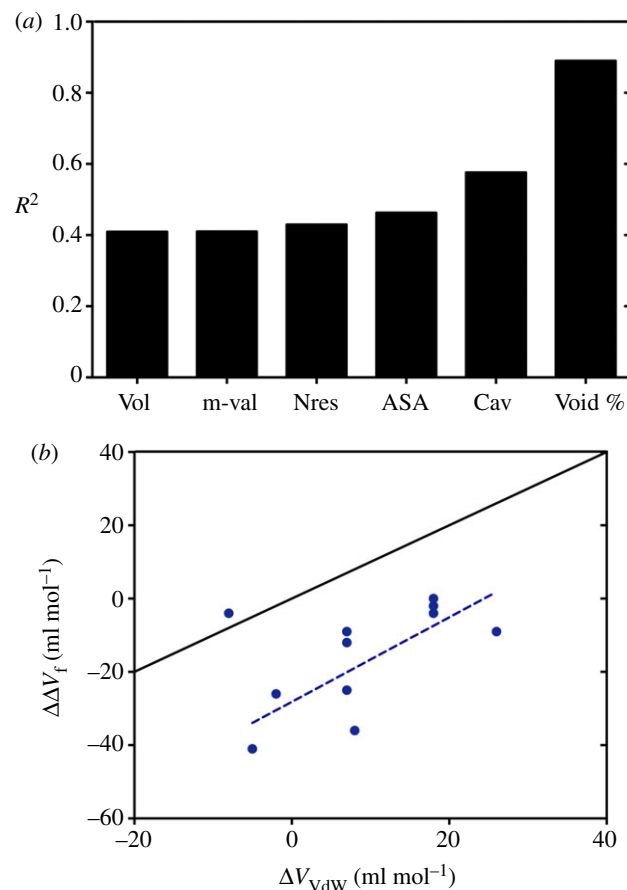


Figure 5. Origin of the volume change for unfolding. (a) Correlation coefficient between the published volume change for unfolding and various properties of a series of proteins. The internal cavity volume (CAV), the number of residues (NRes), the molecular volume (Vol), the m -value from chemical denaturation, the change in ASA upon unfolding and the void volume/molar volume ($V\%$). Proteins are BdpA (Roche and Royer, unpublished data), Cl2 [96], CspB [97], ubiquitin, P13 [98], two azurin mutants (AzI7A and AzF110S) [99], lysozyme [100], a series of Snase Δ + PHS cavity mutants (I92A, V66A, F34A, L38A, L103A, V74A, L25A and L36A) [22] and WT Snase and a series of cavity mutants V66G, V66A and V66 L [88]. (b) Correlation between the measured difference in volume change of folding, $\Delta\Delta V_f$, with respect to the difference in van der Waals volume for a series of Δ + PHS Snase mutants in which buried hydrophobic residues (I, L, V) have been replaced by ionizable residues (D, E, K, R). The black line is simply the difference in van der Waals volume versus the difference in van der Waals volume for each mutation (a line with a zero intercept and a slope of unity). (Online version in colour.)

the packing efficiency or solvent excluded void volume of the proteins tested (figure 5a). By contrast, there is very poor correlation of ΔV_u with protein size or denaturant m -value, indicating poor correlation with the change in ASA upon unfolding. Thus, solvent density changes upon protein hydration do not appear to contribute significantly to the value of ΔV_u . However, the phenomenon of electrostriction, the density of water around charged residues is higher than its density in the bulk, is well known. Thus, while the preponderance of void volume in determining the magnitude of ΔV_u was reasonably well accepted by the community, some interrogation remained, since electrostriction of charged residues would be expected to have a non-negligible and negative contribution to the value of ΔV_u . For this to be the case, the charges would have to be either absent or not hydrated in the folded form of the protein, and present and

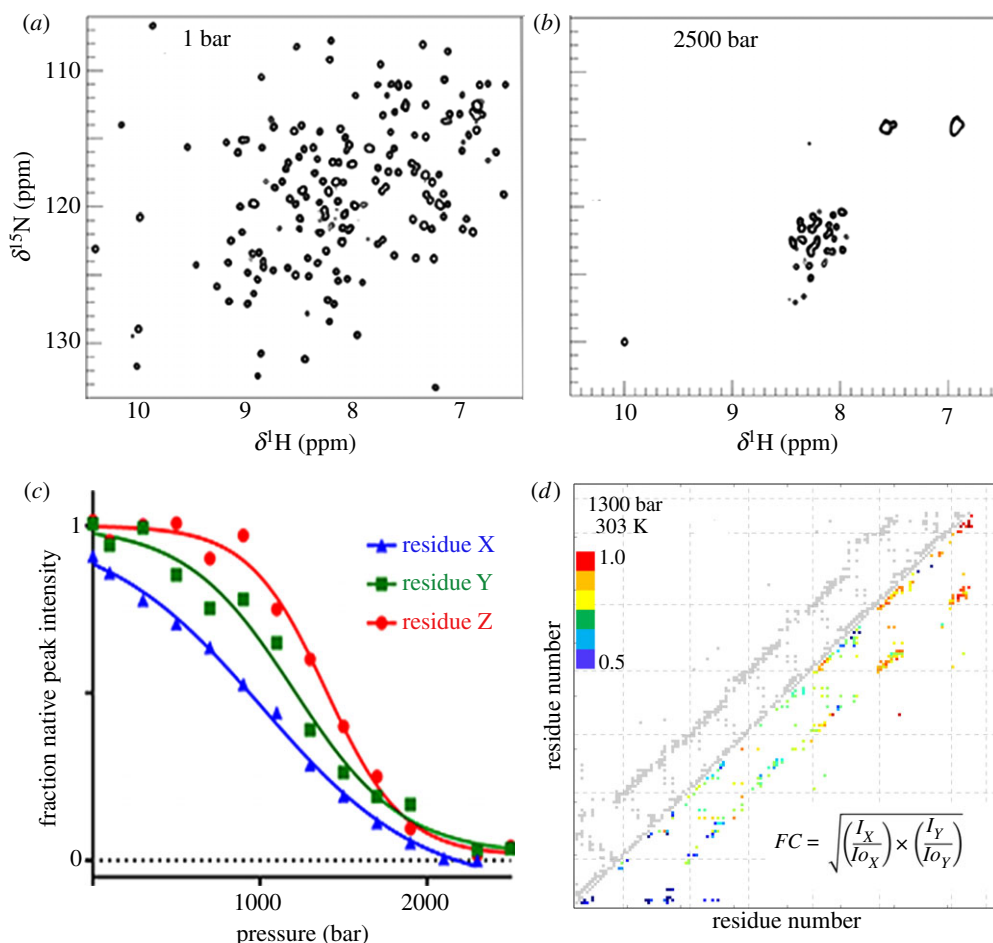


Figure 6. Pressure-dependent HSQC experimental approach. (a) HSQC spectrum of WT pp32 at 293 K and 1 bar, (b) HSQC spectrum of WT pp32 at 293 K and 2500 bar, (c) example curves for the loss of native state peak intensity as a function of pressure. Curves from three of the 155 residues are shown and labelled as residue X, Y and Z, simply for illustrative purposes. (d) Fractional contact histogram for WT pp32 at 1300 bar and 303 K as calculated from the fractional intensity values for each native contact according to the equation in the inset. Native contacts are in grey above the diagonal. (Online version in colour.)

solvated in the unfolded form. Completely buried and non-solvated charge residues being rather rare in proteins, one could argue that in the cases studied to date, this effect was minimal. However, we were rather lucky to have studied for other reasons, in collaboration with Bertrand Garcia-Moreno, a series of variants of Snase with mutations of internal hydrophobic residues to ionizable ones (lysine, histidine, aspartate and glutamate) [101,102]. Crystal structures of some of these residues indicated that the buried groups were not hydrated [103], and pKa measurements indicated that they were uncharged as well [73,104]. Although we did not report it at the time, we found a negative offset of 24 ml mol⁻¹ in the correlation between the measured value of ΔV_u and the expected value based on the volume of the mutated residue (figure 5b). This correlation plot of the data from the above cited experiments indicates that in cases where buried, non-hydrated ionizable or charged residues exist within a folded protein structure, electrostriction of their charges upon unfolding contributes -24 ml mol⁻¹ to ΔV_u .

8. Using pressure and NMR to explore protein folding landscapes

Beyond their use in defining internal solvent excluded cavities as the major contributing factor to the volume change of unfolding of proteins, the three model systems in figure 2 have allowed exploration of the structural and energetic

properties of their folding landscapes and the effects of amino acid substitutions thereon [22,23,31,87,94,105–107]. The combination of pressure perturbation with multidimensional NMR, as well as SAXS, FTIR, fluorescence and coarse-grained molecular dynamics simulations, have provided exquisite structural and energetic details of the conformations and energetics of intermediates in the folding of these three proteins.

8.1. The approach

For the model proteins in figure 2*a,c*, we have used two dimensional ¹⁵N–H heteronuclear single quantum coherence (HSQC) spectra to assess the degree of native structure as a function of pressure. Because the stability of some of the variants of these proteins was high, chemical denaturants were employed to allow for unfolding in the range of the commercial pressure cell (2500 bar). We note that newer cells are now available that reach 3000 bar. We verified by fluorescence that denaturant did not modify the ΔV_u value for global unfolding, but only decreased stability [22,94]. The ¹⁵N–¹H HSQC spectrum of a folded protein (in the range of 7–10 ppm in the proton dimension and 110–130 ppm in the nitrogen dimension) features a large number of well-dispersed peaks, corresponding to the amide NH groups for every amino acid in the protein's sequence, in addition to some side-chain NH groups for histidine, tryptophan, lysine and arginine (e.g. figure 6*a*). The unfolded state, on

the other hand, exhibits a collapsed ^{15}N - ^1H HSQC spectrum such as that in figure 6*b*, with all the amide NH peaks concentrated in a region between 8–9 (^1H) and 120–130 (^{15}N) ppm and the lysine and arginine side chain NH resonances between 7–8 (^1H) and approximately 115 ppm (^{15}N). The unfolded state tryptophan peak is visible, near 10 and 130 ppm for ^1H and ^{15}N , respectively. These conformations exist in slow exchange relative to the NMR timescale such that for a two-state transition, the intensity lost in the native state peaks as the protein unfolds is recovered directly in the unfolded state peaks. Unfortunately, because of the low dispersion, assignment of these unfolded state peaks was not possible, with the exception of the tryptophan residue (for both Snase and pp32). We note that while we monitored the peak volume (rather than the peak intensity), we did not observe any pressure-dependent broadening of the native state peaks. They shift with pressure (as they do with temperature or any other physical parameter (salt, pH, etc.)), and these shifts have been widely used to infer subtle structural changes in protein folded states by pressure (e.g. [108]). The complete backbone assignment of a pressure-denatured state, allowing a systematic comparison of the intensity decrease of each folded cross-peak and the intensity increase of the corresponding unfolded cross-peak was later achieved for the HIV protease.

For both of our model proteins, Snase and pp32 and several of their variants, the loss of the native state HSQC peaks as a function of pressure was monitored. An example showing pressure dependent peak intensity profiles for three residues of pp32 is shown in figure 6*c*. In this particular case, there was a significant spread in the unfolding profiles monitored at all residues, exemplified by these three, indicating that unfolding did not conform to a two-state transition. Note that even while the global unfolding of the protein did not conform to a two-state transition, *locally*, the loss of each individual native state amide HSQC peak as a function of pressure is by definition two-state. For each molecule in the ensemble under any condition, each individual amide senses its native environment, or it does not. Thus, fitting these residue-specific pressure-induced unfolding profiles to a two-state model yields *local* values for ΔG_u and ΔV_u . These represent the free energy and volume changes between the native state and the lowest free energy ensemble of structures in which that particular amide is not in its native environment. And because these transitions are observed with pressure perturbation, this means that the volume differences between the native state and these intermediates is significant, i.e. they contain significantly less solvent excluded void volume than the native state.

Using a combination of HP and NMR, we were able to populate and detect folding intermediates at equilibrium. It was therefore of interest to generate a structural picture of the folding pathway. One convenient approach for visualizing protein structure is to calculate the native state contact map, which we do using the SMOG server [109]. For example, the native contact map for pp32 is shown in the grey pattern above the diagonal in figure 6*d*. Working on the Snase cavity variants [22], we created fractional contact maps at each pressure for each of the variants, based on the fractional intensity values in the pressure-dependent HSQC profiles, an approach later slightly modified in the work on pp32 [105]. These fractional contact maps provide a clear representation of the relative degree of native structure in

different regions of the protein at any given pressure. For example, using the curves in figure 6*c*, assuming that a contact exists between residue X and residue Y in the native structure, the fractional probability of that contact at a given pressure, e.g. 1300 bar, is calculated as the geometric mean of the fractional intensity of residues X and Y (figure 6*d*). The fractional contact map in figure 6*d* corresponds that of the linear repeat protein pp32 at 1300 bar and 303 K. It can be seen in this example that while the N-terminus of pp32 is 50% unfolded under these conditions, the C-terminal repeat and capping motif remain nearly fully folded, with a gradient of native structure in between.

While these fractional contact maps provide useful structural insight, they are not themselves, three dimensional structures, nor do they yield quantitative relative stabilities for the different states populated on the folding landscape. To obtain a more detailed view, the values of the fractional contacts at any given pressure can be used to constrain structure-based models (Go-model) [22]. In this approach, over 100 contact lists are created. Each native contact is present across the ensemble of lists at the fractional level extracted from the pressure-dependent HSQC profiles. This is achieved by using a random number generator for values between 0 and 1. For each contact in each list, the contact is accepted if the random number is lower than its experimental fractional contact value or rejected if it is higher. Then these contact lists are used to run coarse-grained C_α molecular dynamics simulations for 100 ns, and configurations from the last 50 ns are retained. Three hundred lists result in over 30 million configurations which are mapped back to all atom representations [110], and the RMSD with respect to the folded structure and the fraction of native contacts, Q , are calculated for each configuration (figure 7*a*). Cluster analysis is carried out for given bins of Q -values, and the structure from each sub-ensemble showing the lowest RMSD with respect to the others is identified (e.g. Snase $\Delta + \text{PHS}$ in figure 7*b*). From the number of configurations with a given Q -value, pseudo-free energy profiles are constructed (figure 7*c,d*). Examples are given for Snase $\Delta + \text{PHS}$ in 1.8 M GuHCl at 293 K and 800 bar (figure 7*a,b*), and 0.1, 40, 60 and 800 bar (figure 7*c*), and for pp32 at 900 bar and 303 K, in the presence of 1.4 M urea (figure 7*d*).

8.2. Mapping folding landscapes: Snase

The pseudo-free energy profiles derived from the simulations constrained by HP NMR data for Snase $\Delta + \text{PHS}$ as a function of pressure (figure 7*a–c*) revealed the existence of an intermediate ensemble in which the C-terminal helix of the protein was disordered, while the OB fold region remained intact. These results were consistent with several prior studies of Snase folding using native-state hydrogen exchange [111,112] and denaturant-induced unfolding kinetics for WT Snase [113–115], thus validating our approach. We then sought to explore how the introduction of internal cavities would modify the folding landscape of this protein, using the hyperstable $\Delta + \text{PHS}$ variant to engineer the cavities [22,87,107]. Here we focus on the comparison between two of these variants, L125A and I92A. Leucine 125 is found in the C-terminal helix (figure 3*a*), the least stable subdomain of the protein, which is disordered in the folding intermediate ensembles in figure 7*c*. Isoleucine 92 is found in the β -barrel (figure 3*a*), the most stable region of the protein, exhibiting

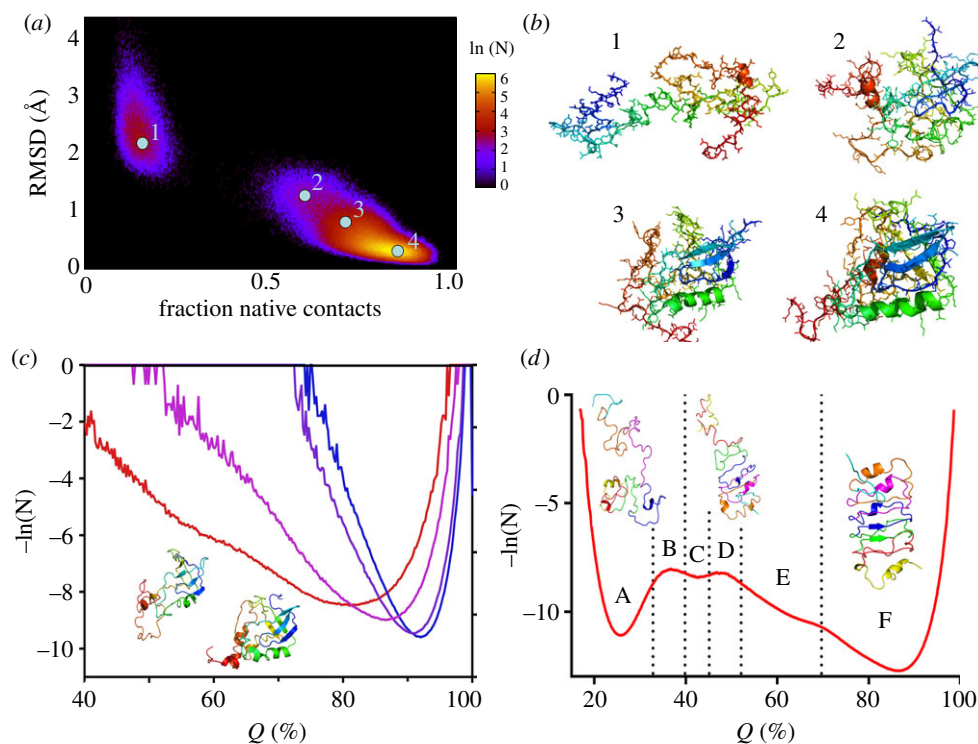


Figure 7. Conformational landscapes from structure-based simulations constrained by HP-NMR data. (a) RMSD versus Q (fraction of native contacts) heat map of the 10 million configurations obtained from the constrained simulations of Snase Δ + PHS at 800 bar and 293 K as described in [22]. (b) Examples of configurations of Snase Δ + PHS from the regions of the heat map in (a), labelled as indicated. (c) Pseudo free energy profile using the number of configurations at all Q -values in (a), $-\ln(N)$, at atmospheric pressure (blue), 400 bar (purple), 600 bar (pink) and 800 bar (red). (d) Pseudo free energy landscape of pp32 at 293 K and 900 bar in 1.4 M urea obtained from constrained structure-based simulations as described in [105]. Structures represent the centroids of cluster analysis of the conformations in the indicated Q regions. (Online version in colour.)

the slowest native state hydrogen exchange [111]. Substitution of these two residues by alanine, thereby creating a cavity, was shown to result in nearly identical degrees of destabilization with respect to the Δ + PHS variant, 3.8 ± 0.1 and 4.0 ± 0.3 kcal mol⁻¹, respectively, for the L125A and I92A mutations [107]. Chemical shift perturbation mapping showed significantly larger perturbations for the L125A variant than for I92A (figure 8) [107], indicating that the less stable C-terminal subdomain is able to better adjust its structure in response to the mutation.

We carried out HP unfolding and HP hydrogen exchange on these two cavity-containing variants, as well as on the Δ + PHS variant [22,87]. In addition to resulting in larger values of ΔV_f , as expected, the mutations modified the width of the distribution of ΔV_f and ΔG_f (figure 9*a,b*) [87], indicating they had an effect on the degree of deviation from two-state unfolding. While the widths of the ΔG_f distribution of values were similar for the Δ + PHS variant and L125A [87], that observed for the I92A variant was much broader. The widths of the distributions of ΔG_f and ΔV_f values was narrowest for L125A and broadest for I92A (figure 9*a,b*), indicating significant heterogeneity in the unfolding of I92A. Pressure-dependent hydrogen exchange on the variants also revealed differences in their conformational landscapes. Exchange from many residues in the Δ + PHS variant was too slow to measure, and hence there are many gaps in the plots of ΔV_x and ΔG_x (figure 9*c*) for this variant. None of the measured values for ΔG_x reached the global stability of this protein, 12 kcal mol⁻¹, indicating that exchange occurred from local opening transitions, all of which had a ΔV_x value consistent with solvent exposure of about two-thirds of the

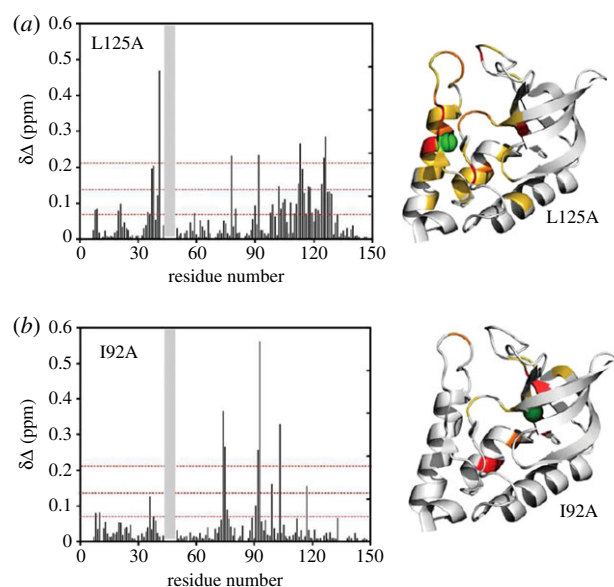


Figure 8. Chemical shift perturbation mapping of Snase Δ + PHS I92A and L125A relative to WT Δ + PHS. (Left) Difference in chemical shift, $\Delta\Delta$, between Snase Δ + PHS L125A and WT Δ + PHS (a) and between Snase Δ + PHS I92A and WT Δ + PHS (b); $\sigma < \Delta\Delta < 2\sigma$, $2\sigma < \Delta\Delta < 3\sigma$ and $\Delta\Delta > 3\sigma$ are coloured in yellow, orange and red, respectively. Data are taken from [107]. Grey bars are placed in the position of the WT Snase residues that are deleted in the Δ + PHS hyperstable variant. (Online version in colour.)

internal void volume, $\Delta V_x/\Delta V_f \sim 0.66$. The L125A variant showed similar patterns of ΔG_x , although a few residues exchanged with the same free energy change as the global

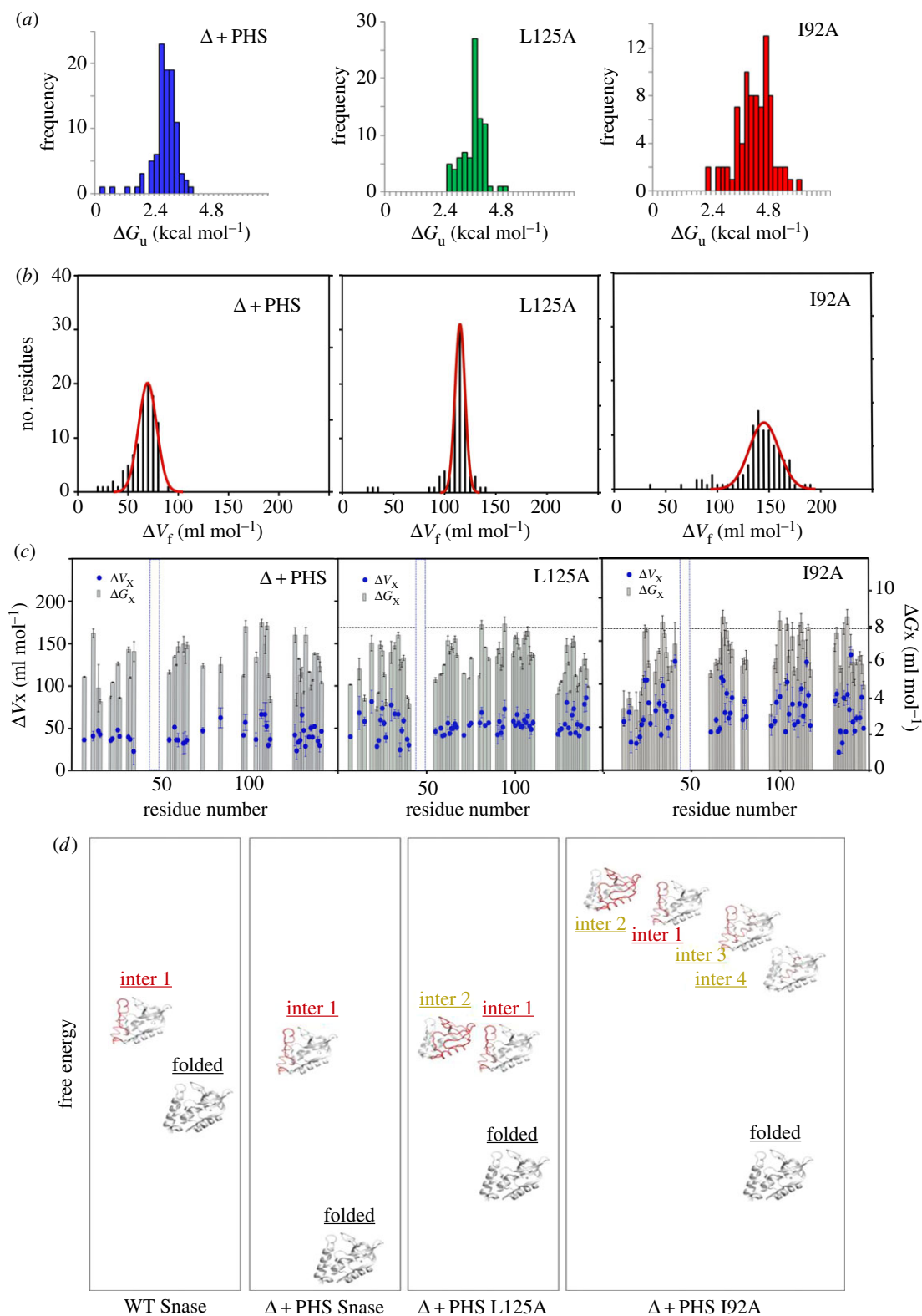


Figure 9. Effect of cavity creating mutations on the pressure response of Snase $\Delta + \text{PHS}$. (a) Distribution of residue-specific free energy changes of unfolding, ΔG_u , from HSQC detected pressure-induced unfolding for (left) WT Snase $\Delta + \text{PHS}$ at 1.8 M GuHCl, (centre) $\Delta + \text{PHS}$ L125A at 0.75 M GuHCl and (right) $\Delta + \text{PHS}$ I92A at 0.75 M GuHCl. (b) A distribution of residue-specific volume changes of folding, ΔV_f , from HSQC detected pressure-induced unfolding for (left) WT Snase $\Delta + \text{PHS}$ at 1.8 M GuHCl, (centre) $\Delta + \text{PHS}$ L125A at 0.75 M GuHCl and (right) $\Delta + \text{PHS}$ I92A at 0.75 M GuHCl. (c) A distribution of residue-specific free energy changes of exchange, ΔG_x (grey bars) and volume changes of exchange, ΔV_x (blue circles) from pressure-dependent H/D exchange experiments for (left) WT Snase $\Delta + \text{PHS}$, (centre) $\Delta + \text{PHS}$ L125A and (right) $\Delta + \text{PHS}$ I92A. (d) Schematic diagram of the intermediate conformational states for WT Snase, Snase $\Delta + \text{PHS}$, $\Delta + \text{PHS}$ L125A and $\Delta + \text{PHS}$ I92A. All data are taken from [87]. (Online version in colour.)

unfolding of this variant. The patterns for ΔV_x were also similar to $\Delta + \text{PHS}$, with the exception of additional heterogeneity in the N-terminus, indicating another intermediate disrupted in this region. The values of ΔV_x , except for a few residues in the N- and C-termini, were less than half

that of the ΔV_f value, indicating that these local unfolding transitions individually do not expose the majority of solvent excluded void. Finally, many more residues in the I92A variant exchanged with global unfolding free energy, and both the ΔV_x and ΔG_x values were highly heterogeneous, as

were the values for ΔV_f . This behaviour is indicative of multiple intermediates with distinct structural properties, and a rather chaotic conformational landscape. For all three variants, the heterogeneity in ΔG_f and ΔV_f values decreased with increasing denaturant [87]. This was our first hint that the folding landscapes sampled in pressure denaturation could be quite different from those observed in urea titrations, and that chemical denaturants had a smoothing effect on the folding landscape.

Altogether these experiments led us to hypothesize the free energy and structural landscapes in figure 9*d*. WT Snase and Δ + PHS Snase both unfold through a single, well-known intermediate ensemble that is disrupted in its C-terminal helix. Δ + PHS L125A unfolds via the same pathway, but also exhibits an intermediate with some disorder in the N-terminus. This is an interesting observation given that the mutation is in the C-terminus and suggests allosteric coupling between these two regions. The I92A variant, on the other hand appears to unfold via multiple and structurally mutually exclusive pathways. These observations serve to highlight the fact that although natural protein sequences, to the extent that reported studies can be generalized, appear to fold via a single well-defined pathway [3], a single amino acid substitution in the appropriate position can lead to funnel-like behaviour. (See also the discussion on p-jump kinetics below.) This suggests that the relative stabilities of all possible conformations in a protein conformational ensemble are not wildly different, and that modest (approx. 4 kcal mol⁻¹) perturbations to these relative stabilities can significantly alter the population distribution. This situation is not surprising, since even global protein stability is not high. We note that such an observation was possible in the context of the Δ + PHS variant because its global stability (12 kcal mol⁻¹) was high enough for the engineering of relatively stable cavity containing variants.

8.3. Mapping folding landscapes of a repeat protein

Folding cooperativity, defined here as the degree to which equilibrium (un)folding corresponds to a two-state transition, is somewhat simpler to conceptualize and interpret for linear repeat proteins which lack sequence distance contacts. We have recently applied our HP NMR approach to investigate the effects of capping [116] and cavities [117] on the folding cooperativity of the pp32 leucine-rich repeat protein (figure 2*c*). Wild-type pp32 was shown to unfold fairly cooperatively under pressure, although intermediates could be detected (figure 7*d*), especially at higher temperature (figure 10*a*) [105]. The fractional contact histograms in figure 10 are colour coded by repeat (as in the inset in figure 10*a*). A fully folded protein presents all native contacts at 100%, but as pressure is increased the histogram of fraction of native contacts shifts to lower values (to the left). The distribution broadens as well, in part due to experimental uncertainty and in part due to deviations from two-state behaviour. The fractional contact histogram for WT pp32 at 293 K and 900 bar in figure 10*a* is broadened beyond experimental uncertainty. Moreover, it is slightly asymmetric, with the yellow and red (N-terminal) contacts shifted to lower values than the rest, indicating lower stability for the N-terminal capping motif and the first repeat. The distribution broadens and this shift is accentuated at higher temperature, implicating also contacts in repeat 2 (green).

Thus, there is an underlying stability gradient in WT pp32, increasing from the N- to the C-terminus. These results are consistent with those obtained from fluorescence-detected urea-induced unfolding kinetics which demonstrated that the most stable part of the protein, and the first to fold, is the C-terminal capping motif (C-cap) and the fifth repeat [84].

Capping motifs are known to increase the global stability of repeat proteins [118–120]. We were interested in the contributions of capping motifs to the features of the folding landscapes of repeat proteins [116]. In the context of the pp32 stability N- to C-terminal gradient, destabilizing mutations in the highly stable C-cap (pp32 Y131F/D146 L, YFDL) led to more cooperative HP unfolding than observed for WT pp32 (figure 10*b*) because destabilization of the stable C-terminus equalized the local stability across the protein. By stark contrast, deletion of the N-terminal capping motif (Δ N-cap) vastly accentuated the stability gradient already present in the WT protein, resulting in very strong deviation from two-state unfolding under pressure (figure 10*c*). The protein appears to unfold in almost a bipartite manner, the fourth repeat (purple) acting as a border between the two N- and C-terminal halves. Correlation of the positions of the residues in repeat 4 with their apparent stability suggested that the ‘unfolded’ residues retained their structure, yet had lost the intensity in their native state peaks because disruption of the N-terminal region leads to a different and heterogeneous chemical environment. In such cases, the native state peak intensity is lost, but no new peaks appear elsewhere in the spectrum because due to heterogeneity they are below the detection limit. These intermediates involving disruption in the N-terminal half of the protein, yet retaining native structure in the C-cap and fourth and fifth repeats bear the hallmarks of molten globule-like structures. Similar observations have been made for the native state HSQC peaks in cold denatured ubiquitin [121]. Comparison of the pressure-dependent increase in the intensity of the unfolded state peaks for the methyl groups of valine, leucine and isoleucine in the 1D proton spectrum (approx. 0.85 and 0.92 ppm) with the loss of native state amide HSQC peak intensity indicated that the intermediates retained considerable core packing. The loss of the folded state indole NH resonance of tryptophan 155, located in the extreme C-terminus of the protein, correlated exactly with the gain in the unfolded state peak intensity for that residue, confirming two-state unfolding in the C-terminus which was not complete by 2500 bar. Fits of these data yielded a rather small volume change and indicated complete unfolding would be achieved by 3500 bar. Thus, comparison of all of these NMR observables indicates that unlike CD-detected urea unfolding of the pp32 Δ N-cap variant, pressure-induced unfolding leads to the population of multiple molten globule intermediates of varying stability and structural disruption.

8.4. Differences between pressure- and urea-induced unfolding

The local (repeat averaged) free energy of the observed transitions for Δ N-cap under pressure increased from the N- to the C-terminus (figure 11*a*, left), but all were less than half the value obtained from CD-detected urea melts (4.13 kcal mol⁻¹) [85], indicating the ensembles reached in the pressure experiments were more stable (closer to native

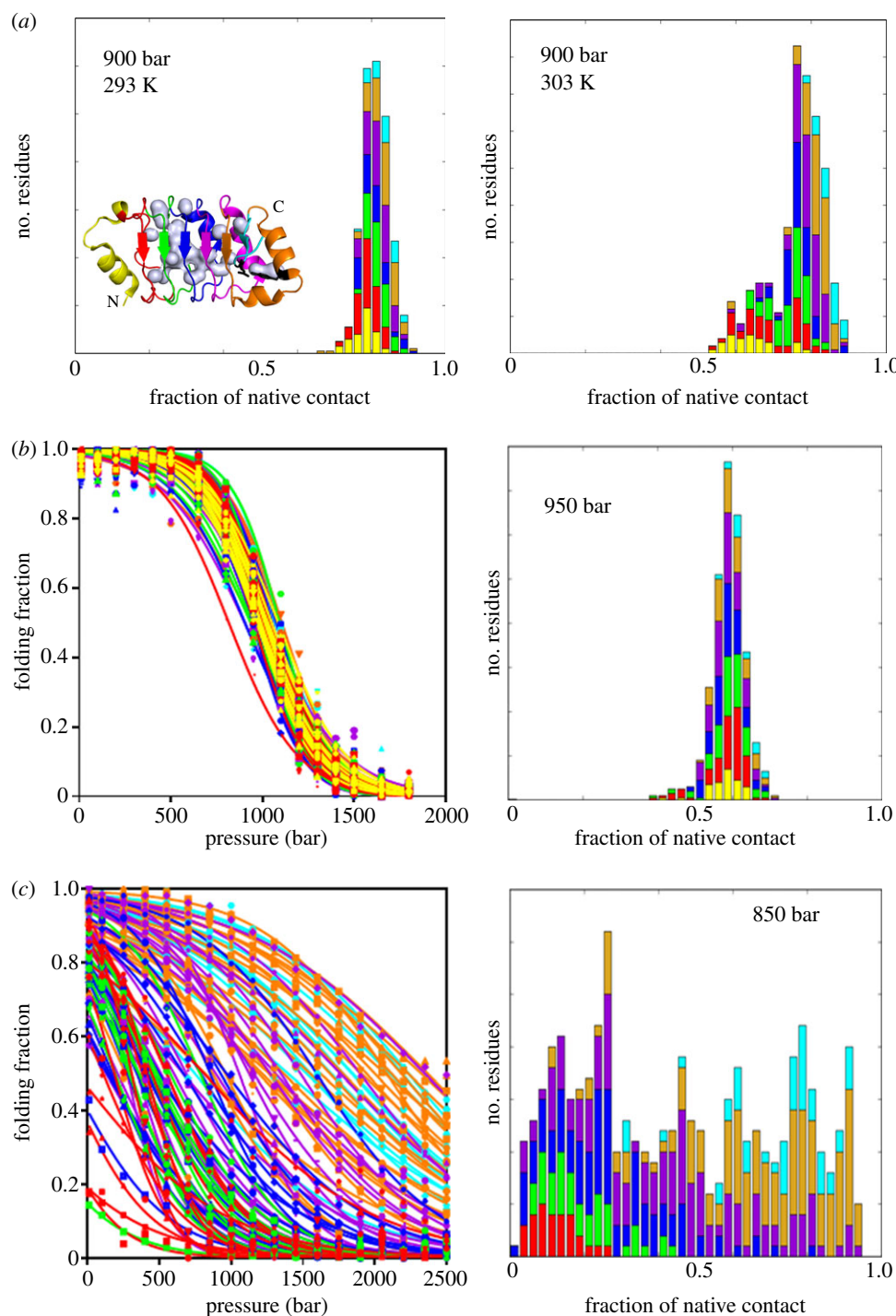


Figure 10. Results of HSQC-detected unfolding of pp32 and capping variants. (a) Fractional contact histograms of WT pp32 at 1.4 M urea and (left) 900 bar and 293 K and (right) 900 bar and 303 K. Inset on left graph, schematic of WT pp32 structure coloured per repeat. All data are taken from [105]. (b) HSQC-detected unfolding of the pp32 YFDL variant (destabilized in the C-terminal capping motif) at 293 K and 0.5 M urea. (Left) Normalized pressure-induced loss of native state amide NH peak intensity for all residues in the pp32 YFDL variant and (right) fractional contact histogram of pp32 YFDL at 950 bar and 0.5 M urea. Contacts are coloured per repeat according to the colour scheme in the inset in (a, left). Data are from [116]. (c) HSQC-detected unfolding of the pp32 Δ N-cap variant (destabilized in the C-terminal capping motif) at 293 K. (Left) Normalized pressure-induced loss of native state amide NH peak intensity for all residues in the pp32 Δ N-cap variant and (right) fractional contact histogram of pp32 Δ N-cap at 850 bar. Contacts are coloured per repeat according to the colour scheme in the inset in (a, left). Data are from [116]. Note that the N-terminal capping motif (yellow) is not present in this variant. (Online version in colour.)

state stability) than those reached in the urea melt. This apparent energetic discrepancy prompted us to perform urea-induced unfolding experiments, monitoring the HSQC spectra as for HP NMR. We found that the urea-induced unfolding also deviated strongly from two-state behaviour, when residue-specific observables were monitored. The difference between the gradient of free energy obtained by NMR (figure 11a, right) and the highly cooperative unfolding

by CD indicated that the intermediates retained secondary structure, yet had lost their native state amide HSQC peaks, corresponding to molten-globule-like intermediates. Only the free energy change observed for residues in the C-terminal capping motif was equivalent to that obtained from analysis of the CD-detected urea unfolding profiles of Δ N-cap, consistent with the complete unfolding of the protein at the highest urea concentrations tested.

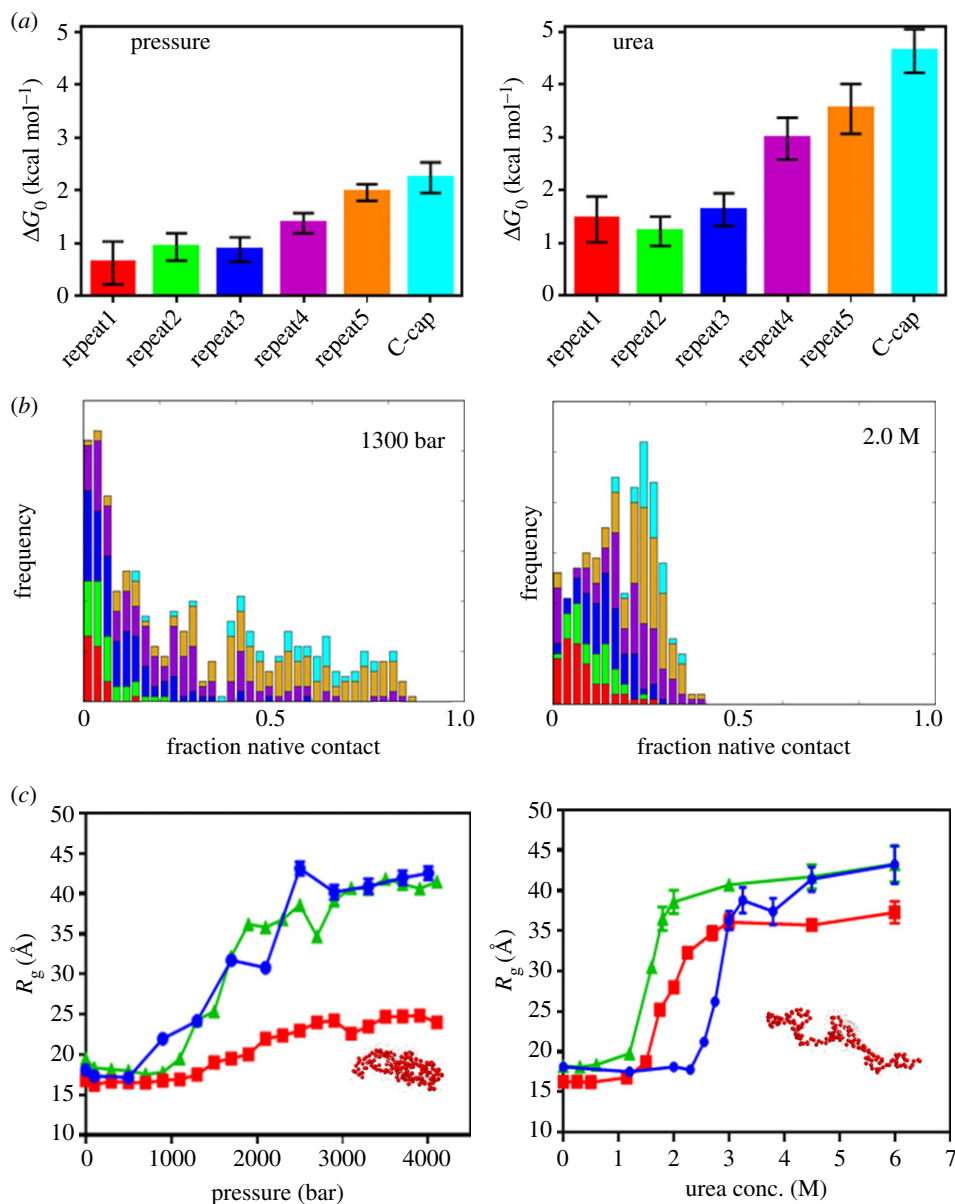


Figure 11. Comparison of pressure and urea denaturation of pp32 Δ N-cap. (a) Average free energy of unfolding per repeat, ΔG_u , from HSQC detected (left) pressure-induced unfolding and (right) urea-induced unfolding of pp32 Δ N-cap as described in [116]. (b) Fractional contact histograms for pp32 Δ N-cap at (left) 1300 bar and (right) 2 M urea. Contacts are colour coded as in figure 10. (c) Comparison of radius of gyration, R_g , for (left) pressure- and (right) urea-induced unfolding of WT pp32 in 1.4 M urea (blue), pp32 YFDL in 0.5 M urea (green) and pp32 Δ N-cap (red). R_g values were calculated from the pair distribution functions, $P(r)$ as described in [116]. (Inset on left is a bead model of pp32 Δ N-cap at 4.1 kbar and the inset on the right is a model of WT pp32 in 6 M urea obtained as described in [116].) (Online version in colour.)

While unfolding of the Δ N-cap variant of pp32 deviated from two-state behaviour in both HP and urea-induced unfolding, the repeat averaged local free energy changes were all larger in urea than under pressure (compare left and right in figure 11a). Moreover, comparison of the fractional contact histograms at an average of approximately 75% unfolded reveals structural differences in the intermediates (figure 11b). Under pressure there is a broad gradient of contact probability for the fifth repeat and the C-cap, whereas this spread is much smaller in urea. This persistence of structure in the C-terminus under pressure indicates very small and non-uniformly distributed volume changes associated with disruption of this region which exacerbate the underlying stability gradient, leading to persistence of structure. By contrast, surface area (the basis for urea denaturation) is equally distributed across the structure.

We also characterized the overall shape of the proteins (WT pp32, the YFDL mutant destabilized in the C-cap and Δ N-cap) by SAXS as a function of pressure and urea. Owing to their higher stability, the HP SAXS experiments on WT and YFDL were carried out in the presence of 1.5 and 0.5 M urea, respectively, whereas no urea was used in the HP SAXS experiments on the Δ N-cap variant. WT pp32 and YFDL exhibited the same radius of gyration (R_g) at both the highest pressures and highest urea concentrations (figure 11c). This R_g value which was consistent with a random coil structure (see inset in figure 11c, right). The Δ N-cap variant exhibited an R_g value at the highest urea concentration consistent with a random coil of the length of this deletion variant. By contrast, because the HP SAXS experiments on Δ N-cap were carried out in the absence of denaturant, the protein remains fairly collapsed (see inset in

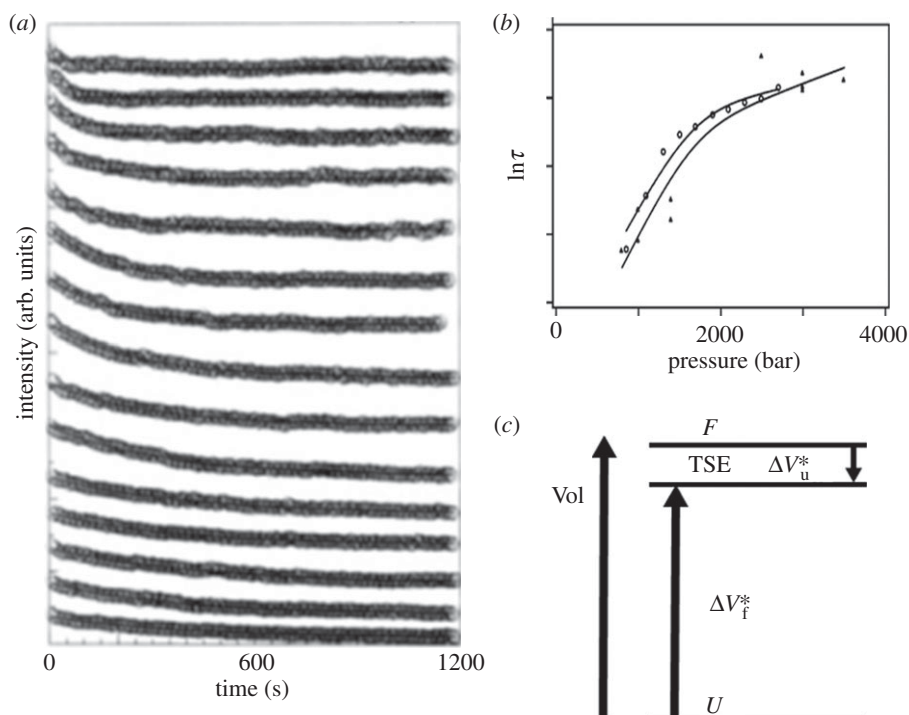


Figure 12. Pressure-jump kinetics on WT Snase. (a) Fluorescence intensity of the single tryptophan of WT Snase (Trp 140) as a function of time after pressure jumps. Top curve is at 930 bar; bottom curve is at 2500 bar. Jumps are approximately 100–150 bar. Adapted from [122]. (b) Pressure chevron plot of the natural logarithm of the relaxation time versus pressure for WT Snase. Circles are values of $\ln \tau$ obtained from fluorescence-detected p-jumps [122] and triangles are from SAXS detected p-jumps as described in [123]. (c) Volume diagram for the kinetics of WT Snase folding. F is folded state, U is unfolded state and TSE is transition state ensemble. The activation volume for folding, ΔV_f^\ddagger , is positive while that of unfolding, ΔV_u^\ddagger , is negative. The total difference in volume corresponds to the equilibrium volume change, ΔV_f^0 .

figure 11c, left), even at pressures that largely exceed those used in the NMR experiments (4 kbar compared to 2.5 kbar), and at which the protein is predicted to be completely unfolded. This residual structure is disrupted by the addition of 1.5 M urea to the WT protein or 0.5 M urea to the YFDL variant. We observed similar behaviour in HP SAXS, fluorescence and FTIR experiments on the Nank protein, with increasing urea leading to more disrupted structures at HP [94].

9. Folding kinetics at high pressure

Another aspect of protein folding landscapes that we have explored over the years is the nature of the transition state ensemble. Originally, we observed in fluorescence detected p-jump relaxation experiments on WT Snase that pressure slowed folding considerably [122]. Data were analysed assuming exponential relaxation rates, τ , as well as classical relaxation kinetics with an exponential dependence of the folding and unfolding rate constants, k_f and k_u , on pressure according to folding and unfolding activation volumes, ΔV_f^\ddagger and ΔV_u^\ddagger , as below:

$$I_t = I_0 e^{-t/\tau}, \quad (9.1)$$

$$k_{\text{obs}} = (k_f + k_u) = \frac{1}{\tau}, \quad (9.2)$$

$$k_f(p) = k_{f0} e^{-p\Delta V_f^\ddagger/RT}, \quad (9.3)$$

where k_{f0} (or k_{u0}) are the values of the folding (or unfolding) rate constants at atmospheric pressure. The relaxation time at any pressure is the inverse of the observed rate constant, k_{obs} . We found that as pressure increased the rate of the decrease in fluorescence intensity of the single tryptophan residue in

WT Snase decreased, the relaxation time increased, such that by 2500 bar relaxation after a pressure jump took nearly 20 min (figure 12a). We note that at atmospheric pressure the unfolding of WT Snase is not a single exponential. This complex kinetic behaviour is largely due to proline isomerization [124]. Given the very slow relaxation under pressure, above 900 bar, the pressure at which the protein began to unfold, proline isomerization was no longer rate limiting. The pressure dependence of logarithm of the relaxation time detected both by HP fluorescence and HP SAXS showed that most of the pressure effect occurred below the pressure midpoint of unfolding (figure 12b), and accordingly, analysis yielded a large positive activation volume for folding and a small negative activation volume for unfolding, nearly indistinguishable from zero. This means that in WT Snase, most of the solvent excluded void volume is present in the transition state ensemble (TSE), i.e. volumetrically the TSE is close to the native state (figure 12c). Similar results have been reported for tendamistat [97] and the chymotrypsin inhibitor 2 [96].

We next wondered how robust these TSEs would be to changes in sequence or conditions. Using several variants of the hyperstable $\Delta +$ PHS Snase with ionizable residues engineered at core positions [103,104] (figure 3a), we carried out fluorescence-detected p-jump relaxation experiments [101,102] (figure 13a–c). The volumetric properties of the transition state were found to depend upon the position of the mutation (figure 13b). If the ionizable residue was placed in a region of the protein which is known to not be ordered at the barrier (L125 K, in the C-terminal helix for example), then the volumetric properties of the TSE were identical to those of WT Snase. However, if the ionizable residue was placed in the central core of the protein, known to be

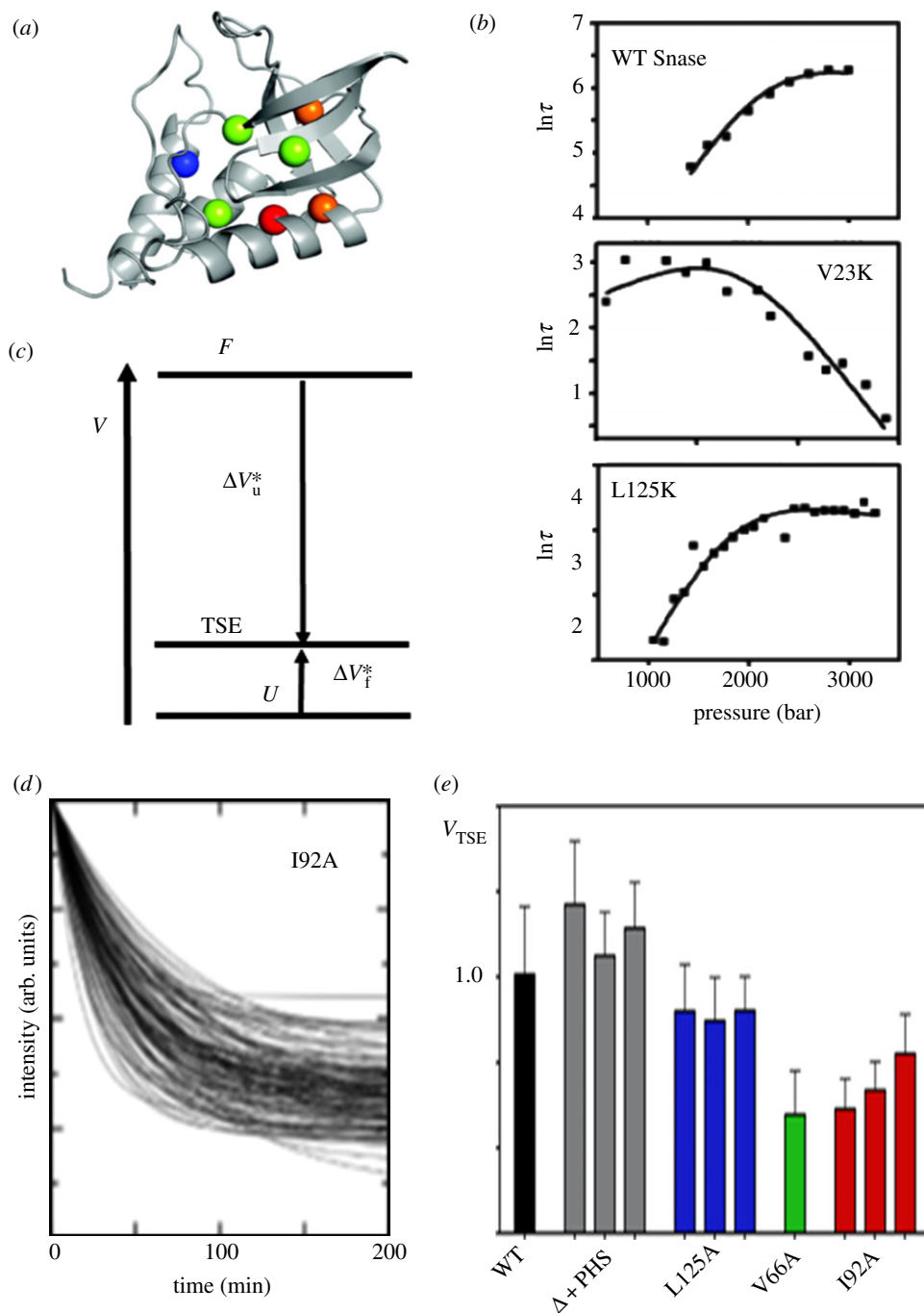


Figure 13. Effect of mutations on the volumetric properties of the TSE of Snase variants. (a) Schematic diagram of Snase with positions of mutations to ionizable residues coloured from blue to red according to their effects on the volume of the TSE. Positions in red exhibited very low volume TSEs relative to WT Snase, while those in blue were indistinguishable from WT Snase TSE volume. (b) Pressure chevron plots for WT Snase, Snase Δ + PHS V23 K and Snase Δ + PHS L125 K. Adapted from [102]. (c) Volumetric diagram of the Δ + PHS V23 K variant. (d) Residue specific p-jump relaxation profiles from time-dependent HSQC spectra of Snase Δ + PHS I92A as described in [64]. (e) Average V_{TSE} (ratio of $\Delta V_u^*/\Delta V_f^*$) for WT Snase, Snase Δ + PHS and several cavity-containing variants as indicated. The value of V_{TSE} is the average of all the residue-specific values obtained from p-jump HSQC or HMQC SO-FAST experiments as described in [64]. Error bars represent the standard deviation for all residues. (Online version in colour.)

ordered in the WT transition state, the volumetric properties of the mutant TSE were quite distinct from those of the WT. In this case, as in the example of the V23 K variant (figure 13*b*), the major effect of pressure was to speed up unfolding, rather than to slow folding, indicating that the TSE was volumetrically quite different from that of the WT protein. In the V23 K variant, relatively little solvent excluded void volume is present in the TSE (figure 13*c*). This substitution destabilized the WT TSE to such an extent that folding proceeded through a different, more open TSE, which in the WT protein is of higher energy. Thus, the

V23 K mutation reorders the high energy states of the protein, modifying the structure at the folding barrier. We found a similar pattern of effects of substitutions on the TSE with the cavity creating mutations in Snase shown in figure 3*a* [64]. Relaxation under pressure was slow enough that we were able to measure HSQC (or SO-FAST HMQC) spectra as a function of time after pressure jumps [64]. This allowed us to monitor time-dependent unfolding at every amide in the proteins. For some of the variants (Δ + PHS, V66A, L125A and I92A), we found very different relaxation rates for different residues (figure 13*d*), indicating funnel-like

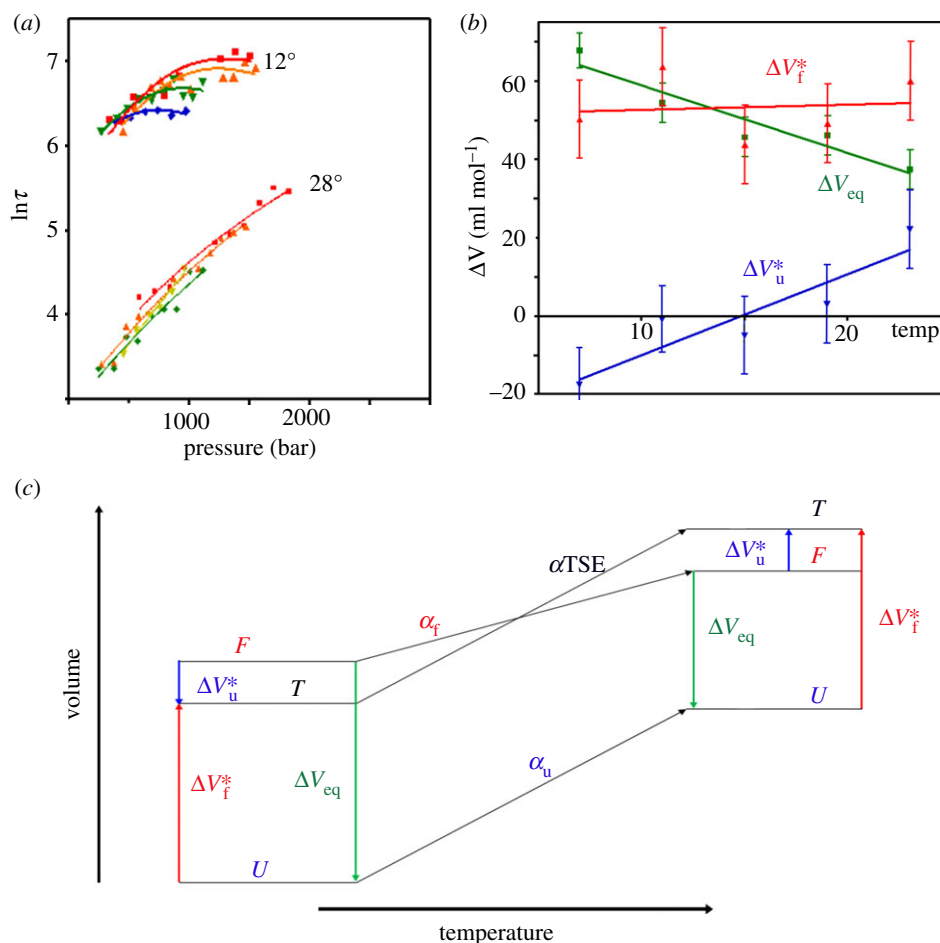


Figure 14. Effect of temperature on the volumetric properties of the TSE of the ankyrin repeat domain, Nank. (a) Pressure chevron plot for Nank at 12 and 28°C. Different colour plots correspond to different urea concentrations increasing from red to blue as described in [94]. (b) Temperature dependence of the activation and equilibrium volume changes for Nank as noted. (c) Schematic of the temperature dependence of the relative volumes of the folded (F), unfolded (U) and transition state ensemble (TSE) for Nank. The coefficients of thermal expansion, α , are larger for the unfolded state and the TSE than for the folded state. (Online version in colour.)

multiple and structurally mutually exclusive parallel folding pathways. By contrast, WT Snase conformed fairly well to a two-state reaction, with very similar kinetics observed for all residues (see figure S4 in [64]). The quantity V_{TSE} , the ratio of the activation volume for folding over the equilibrium volume change, $V_{TSE} = \Delta V_f^* / \Delta V_f^0$ (figure 13e), was calculated from the average volumetric values for all residues for each protein. For WT Snase, the V_{TSE} was near unity, consistent with our earlier fluorescence detected p-jump kinetics results discussed above, and with the notion of a volumetrically native-like TSE. The V66A and I92A variants had much lower values of V_{TSE} , indicating more open structures at the barrier with much less solvent-excluded void volume. In the case of the I92A variant, the flux through the different folding routes was modified by increasing the denaturant concentration. The L125A variant showed values lower than unity, even though the TSE was shown to be similar to that of the WT. The difference in V_{TSE} between the two proteins can be understood in light of the fact that in the L125A variant, an additional cavity is present in the folded structure between the core of the protein and the C-terminal helix. This cavity is not present at the barrier because the C-terminal helix is not ordered. Hence, the L125A V_{TSE} value is entirely consistent with a WT-like TSE.

As discussed in the Introduction, temperature significantly modulates the volume change of unfolding due to the difference in expansivity between the folded and

unfolded states. We were interested in the thermal expansion properties of the TSE. Over 20 years ago, we determined from fluorescence and FTIR-detected p-jump relaxation kinetics experiments at multiple temperatures that the expansivity of the folded state of WT Snase and that of its TSE were nearly identical [45]. The situation was quite different for the Ankyrin repeat protein, Nank (figure 2b). The temperature dependence of the pressure-dependent relaxation times showed interesting behaviour (figure 14a). At low temperature, they took on the curved chevron-type form typical for unfolding by denaturants, indicating that the perturbation slows folding and speeds up unfolding. However, at higher temperature, while the slope of the folding arm of the pressure chevron plot was similar to that at low temperature, the slope of the unfolding arm changed signs. The temperature dependence of the activation volumes for folding, ΔV_f^* , and unfolding, ΔV_u^* , as well as the equilibrium volume change for folding, ΔV_f^0 (figure 14b) revealed that the decrease in ΔV_f^0 was due to the increase in the ΔV_u^* . At low temperature, the TSE was volumetrically close to yet lower than that of the folded state, as for Snase. However, unlike Snase, the expansivity of the Nank TSE, α_{TSE} , was similar to that of the unfolded, α_u , rather than folded state, α_f , such that as temperature increased the TSE volume increased more than that of the folded state (figure 14c). At high temperature, Nank unfolding involved an increase in volume, as did folding, such that both activation volumes

were positive in sign. While the molecular determinants of the expansivity of proteins are largely due to hydration [15], significant differences in expansivity can result from mutations, suggesting that the capacity of the structure itself to expand, thereby increasing internal solvent-excluded void volume is also an important factor [13,30,31]. We hypothesize that the TSE of the Nank protein, while very similar to the folded state, has a higher capacity for expansion because many of the stabilizing interactions are not locked in at the barrier, and hence its expansion is similar to that of the unfolded state. We have found that repeat deletions or cavity-creating mutations in the Nank protein can also lead to a TSE volume that is larger than that of the folded state [23].

10. Future directions

The combination of high hydrostatic pressure with state-of-the-art biophysical techniques allows for in-depth characterization of the structural and energetic characteristics of protein conformational landscapes. Comparison of the results obtained using pressure perturbation with those from temperature, pH or chemical denaturation offers truly comprehensive insight. The physical mechanisms of each of these different perturbations is distinct, leading to distinct effects on folding landscapes. Arguably, none of these perturbation approaches is perfect, because what is desired, but generally unattainable, is to characterize the properties of native states and intermediates under native state conditions. However, the combined information from

all these approaches certainly provides an extensive view of the relative stabilities of different conformational ensembles available to proteins and how these are modulated by sequence and conditions.

Beyond satisfying our curiosity as to the degree of complexity of protein folding landscapes and the role of amino acid sequence in defining their features, what motivates such in-depth studies? One major motivation is a desire to better understand protein conformational transitions that are implicated in function. Hence, moving beyond model systems to interrogate functional conformational equilibria in proteins implicated in human health represents one direction for future studies. Along these lines, protein folding diseases represent an increasing emotional and economic burden on society. Better defining the implication of low, lying excited states and the role of amino acid sequence in modulating their population represents another avenue for the application of HP techniques. Finally, understanding and eventually modulating any chemical reaction requires detailed structural and energetic information about all of the states involved. Precisely because of its lack of structure, the unfolded state has been difficult to adequately describe. It is possible that the combined use of multiple perturbations with multiple observables will help to tease apart the underlying relationships between the energetics and the structures of proteins.

Data accessibility. This article does not contain any unpublished data.

Competing interests. We declare we have no competing interests.

Funding. Funding sources for the work presented in this review were acknowledged in the original articles, cited here.

References

1. Englander SW, Mayne L, Kan Z. 2016 Protein folding—how and why: by hydrogen exchange, fragment separation, and mass spectrometry. *Annu. Rev. Biophys.* **45**, 135–152. (doi:10.1146/annurev-biophys-062215-011121)
2. Englander SW, Mayne L. 2014 The nature of protein folding pathways. *Proc. Natl. Acad. Sci. USA* **111**, 15 873–15 880. (doi:10.1073/pnas.1411798111)
3. Englander SW, Mayne L. 2017 The case for defined protein folding pathways. *Proc. Natl. Acad. Sci. USA* **114**, 8253–8258. (doi:10.1073/pnas.1706196114)
4. Gruebele M, Dave K, Sukenik S. 2016 Globular protein folding *in vitro* and *in vivo*. *Annu. Rev. Biophys.* **45**, 233–251. (doi:10.1146/annurev-biophys-062215-011236)
5. Jagannathan B, Marqusee S. 2013 Protein folding and unfolding under force. *Biopolymers* **99**, 860–869. (doi:10.1002/bip.22321)
6. Bridgman. 1914 The coagulation of albumin by pressure. *J. Biol. Chem.* **19**, 511–512.
7. Silva JLJL, Foguel D, Royer CACA. 2001 Pressure provides new insights into protein folding, dynamics and structure. *Trends Biochem. Sci.* **26**, 612–618. (doi:10.1016/S0968-0004(01)01949-1)
8. Royer CA. 2002 Revisiting volume changes in pressure-induced protein unfolding. *Biochim. Biophys. Acta* **1595**, 201–209. (doi:10.1016/S0167-4838(01)00344-2)
9. Schweiker KL, Makhatadze GI. 2009 *Use of pressure perturbation calorimetry to characterize the volumetric properties of proteins*, 1st edn. Amsterdam, The Netherlands: Elsevier Inc.
10. Mitra L, Smolin N, Ravindra R, Royer C, Winter R. 2006 Pressure perturbation calorimetric studies of the solvation properties and the thermal unfolding of proteins in solution—experiments and theoretical interpretation. *Phys. Chem. Chem. Phys.* **8**, 1249–1265. (doi:10.1039/b516608j)
11. Seemann H, Winter R, Royer CA. 2001 Volume, expansivity and isothermal compressibility changes associated with temperature and pressure unfolding of staphylococcal nuclease. *J. Mol. Biol.* **307**, 1091–1102. (doi:10.1006/jmbi.2001.4517)
12. Lin L-N, Brandts JMF, Brandts JMF, Plotnikov V. 2002 Determination of the volumetric properties of proteins and other solutes using pressure perturbation calorimetry. *Anal. Biochem.* **302**, 144–160. (doi:10.1006/abio.2001.5524)
13. Mitra L, Rouget J-B, Garcia-Moreno B, Royer CA, Winter R. 2008 Towards a quantitative understanding of protein hydration and volumetric properties. *Chemphyschem* **9**, 2715–2721. (doi:10.1002/cphc.200800405)
14. Chen CR, Makhatadze GI. 2015 ProteinVolume: calculating molecular van der Waals and void volumes in proteins. *BMC Bioinf.* **16**, 101. (doi:10.1186/s12859-015-0531-2)
15. Chen CR, Makhatadze GI. 2017 Molecular determinants of temperature dependence of protein volume change upon unfolding. *J. Phys. Chem. B* **121**, 8300–8310. (doi:10.1021/acs.jpbc.7b05831)
16. Chen CR, Makhatadze GI. 2017 Molecular determinant of the effects of hydrostatic pressure on protein folding stability. *Nat. Commun.* **8**, 14561. (doi:10.1038/ncomms14561)
17. Richards FM. 1974 The interpretation of protein structures: total volume, group volume distributions and packing density. *J. Mol. Biol.* **82**, 1–14. (doi:10.1016/0022-2836(74)90570-1)
18. Rashin AA, Iofin M, Honig B. 1986 Internal cavities and buried waters in globular proteins. *Biochemistry* **25**, 3619–3625. (doi:10.1021/bi00360a021)
19. Baase WA, Liu L, Tronrud DE, Matthews BW. 2010 Lessons from the lysozyme of phage T4. *Protein Sci.* **19**, 631–641. (doi:10.1002/pro.344)
20. Matthews BW, Liu L. 2009 A review about nothing: are apolar cavities in proteins really empty? *Protein Sci.* **18**, 494–502. (doi:10.1002/pro.61)
21. Ando N, Barstow B, Baase WA, Fields A, Matthews BW, Gruner SM. 2008 Structural and thermodynamic characterization of T4 lysozyme mutants and the contribution of internal cavities to pressure denaturation. *Biochemistry* **47**, 11 097–11 109. (doi:10.1021/bi801287m)
22. Roche J, Caro JA, Norberto DR, Barthe P, Roumestand C, Schlessman JL. 2012 Cavities

- determine the pressure unfolding of proteins. *Proc. Natl. Acad. Sci. USA* **109**, 6945–6950. (doi:10.1073/pnas.1200915109)
23. Rouget J. 2012 Size and sequence and the volume change of protein folding. *JAM Chem. Soc.* **133**, 6020–6027. (doi:10.1021/ja200228w.Size)
 24. Bianco V, Franzese G, Dellago C, Coluzza I. 2017 Role of water in the selection of stable proteins at ambient and extreme thermodynamic conditions. *Phys. Rev. X* **7**, 1–15. (doi:10.1103/PhysRevX.7.021047)
 25. Ghosh T, Garcia AE, Garde S. 2001 Molecular dynamics simulations of pressure effects on hydrophobic interactions. *J. Am. Chem. Soc.* **123**, 10 997–11 003. (doi:10.1021/ja010446v)
 26. Sarupria S, Garde S. 2009 Quantifying water density fluctuations and compressibility of hydration shells of hydrophobic solutes and proteins. *Phys. Rev. Lett.* **103**, 4–7. (doi:10.1103/PhysRevLett.103.037803)
 27. Hawley SA. 1971 Reversible pressure–temperature denaturation of chymotrypsinogen. *Biochemistry* **10**, 2436–2442. (doi:10.1021/bi00789a002)
 28. Zipp A, Kauzmann W. 1973 Pressure denaturation of metmyoglobin. *Biochemistry* **12**, 4217–4228. (doi:10.1021/bi00745a028)
 29. Meersman F, Smeller L, Heremans K. 2006 Protein stability and dynamics in the pressure–temperature plane. **1764**, 346–354. (doi:10.1016/j.bbapap.2005.11.019)
 30. Dellarole M, Kobayashi K, Rouget J-B, Caro JA, Roche J, Islam MM, Garcia-Moreno E. B, Kuroda Y, Royer CA. 2013 Probing the physical determinants of thermal expansion of folded proteins. *J. Phys. Chem. B* **117**, 12 742–12 749. (doi:10.1021/jp401113p)
 31. Dellarole M *et al.* 2015 Evolutionarily conserved pattern of interactions in a protein revealed by local thermal expansion properties. *J. Am. Chem. Soc.* **137**, 9354–9362. (doi:10.1021/jacs.5b04320)
 32. Wong PTT. 1991 Pressure effect on hydrogen isotope exchange kinetics in chymotrypsinogen investigated by FT-IR spectroscopy. *Can. J. Chem.* **69**, 1699–1704.
 33. Lerch MT, Horwitz J, McCoy J, Hubbell WL, Horowitz J, John M, Wayne LH. 2013 Circular dichroism and site-directed spin labeling reveal structural and dynamical features of high-pressure states of myoglobin. *Proc. Natl. Acad. Sci. USA* **110**, E4714–E4722. (doi:10.1073/pnas.1320124110)
 34. Lange R, Balny C. 2002 UV-visible derivative spectroscopy under high pressure. *BBA-Protein Struct. M.* **1595**, 80–93. (doi:10.1016/S0167-4838(01)00336-3)
 35. Royer CA. 2006 Probing protein folding and conformational transitions with fluorescence probing protein folding and conformational transitions with fluorescence. *Chem. Rev.* **106**, 1769–1784. (doi:10.1021/cr0404390)
 36. Royer CA, Mann CJ, Matthews CR. 1993 Resolution of the fluorescence equilibrium unfolding profile of trp aporepressor using single tryptophan mutants. *Protein Sci.* **2**, 1844–1852. (doi:10.1002/pro.5560021106)
 37. Paladini AA, Weber G. 1981 Pressure-induced reversible dissociation of enolase. *Biochemistry* **20**, 2587–2593. (doi:10.1021/bi00512a034)
 38. Cioni P, Gabellieri E. 2011 Protein dynamics and pressure: what can high pressure tell us about protein structural flexibility? *BBA-Protein Proteom.* **1814**, 934–941. (doi:10.1016/j.bbapap.2010.09.017)
 39. Rietveld AWM, Ferreira ST. 1996 Deterministic pressure dissociation and unfolding of triose phosphate isomerase: persistent heterogeneity of a protein dimer. *Biochemistry* **35**, 7743–7751. (doi:10.1021/bi952118b)
 40. Neumaier S, Kiefhaber T. 2014 Redefining the dry molten globule state of proteins. *J. Mol. Biol.* **426**, 2520–2528. (doi:10.1016/j.jmb.2014.04.022)
 41. Patra S, Anders C, Erwin N, Winter R. 2017 Osmolyte effects on the conformational dynamics of a DNA hairpin at ambient and extreme environmental conditions. *Angew. Chemie. Int. Ed.* **56**, 5045–5049. (doi:10.1002/anie.201701420)
 42. Müller JD, Gratton E. 2003 High-pressure fluorescence correlation spectroscopy. *Biophys. J.* **85**, 2711–2719. (doi:10.1016/S0006-3495(03)74694-3)
 43. Luan B, Lyle N, Pappu R V, Raleigh DP. 2014 Denatured state ensembles with the same radii of gyration can form significantly different long-range contacts. *Biochemistry* **53**, 39–47. (doi:10.1021/bi4008337)
 44. Riback JA *et al.* 2017 Innovative scattering analysis shows that hydrophobic disordered proteins are expanded in water. *Science* **358**, 238–241. (doi:10.1126/science.aan5774)
 45. Panick G, Vidugiris GJ, Malessa R, Rapp G, Winter R, Royer CA. 1999 Exploring the temperature–pressure phase diagram of staphylococcal nuclease. *Biochemistry* **38**, 4157–4164. (doi:10.1021/bi982608e)
 46. Panick G, Winter R. 2000 Pressure-induced unfolding/refolding of ribonuclease A: static and kinetic Fourier transform infrared spectroscopy study. *Biochemistry* **39**, 1862–1869. (doi:10.1021/bi992176n)
 47. Schroer MAM *et al.* 2010 High-pressure SAXS study of folded and unfolded ensembles of proteins. *Biophys. J.* **99**, 3430–3437. (doi:10.1016/j.bpj.2010.09.046)
 48. Krywka C, Sternemann C, Paulus M, Javid N, Winter R, Al-Sawalmih A, Yi S, Raabe D, Tolan M. 2007 The small-angle and wide-angle X-ray scattering set-up at beamline BL9 of DELTA. *J. Synchrotron Radiat.* **14**, 244–251. (doi:10.1107/S0909049507009727)
 49. Ando N, Chenevier P, Novak M, Tate MW, Gruner SM. 2008 High hydrostatic pressure small-angle X-ray scattering cell for protein solution studies featuring diamond windows and disposable sample cells. *J. Appl. Crystallogr.* **41**, 167–175. (doi:10.1107/S0021889807056944)
 50. Peng X, Jonas J, Silva JL. 1994 High-pressure NMR study of the dissociation of arc repressor. *Biochemistry* **33**, 8323–8329. (doi:10.1021/bi00193a020)
 51. Samarasinghe SD, Campbell DM, Jonas J, Jonas A. 1992 High-resolution NMR study of the pressure-induced unfolding of lysozyme. *Biochemistry* **31**, 7773–7778. (doi:10.1021/bi00149a005)
 52. Royer CA, Hinck AP, Loh SN, Prehoda KE, Peng X, Jonas J, Markley JL, Peng X, Jonas J. 1993 Effects of amino acid substitutions on the pressure denaturation of staphylococcal nuclease as monitored by fluorescence and nuclear magnetic resonance spectroscopy. *Biochemistry* **32**, 5222–5232. (doi:10.1021/bi00070a034)
 53. Wagner G. 1980 Activation volumes for the rotational motion of interior aromatic rings in globular proteins determined by high resolution 1 h NMR at variable pressure. *FEBS Lett.* **112**, 280–284. (doi:10.1016/0014-5793(80)80198-0)
 54. Yamaguchi T, Yamada H, Akasaka K. 1995 Thermodynamics of unfolding of ribonuclease A under high pressure. A study by proton NMR. *J. Mol. Biol.* **250**, 689–694. (doi:10.1006/jmbi.1995.0408)
 55. Ehrhardt MR, Erijman L, Weber G, Wand AJ. 1996 Molecular recognition by calmodulin: pressure-induced reorganization of a novel calmodulin-peptide complex. *Biochemistry* **35**, 1599–1605. (doi:10.1021/bi951267r)
 56. Kremer W, Arnold MR, Kachel N, Kalbitzer HR. 2004 The use of high-sensitivity sapphire cells in high pressure NMR spectroscopy and its application to proteins. *Spectrosc. Int. J.* **18**, 271–278. (doi:10.1155/2004/407619)
 57. Korzhnev DM, Bezsonova I, Evanics F, Taulier N, Zhou Z, Bai Y, Chalikian TV, Prosser RS, Kay LE. 2006 Probing the transition state ensemble of a protein folding reaction by pressure-dependent NMR relaxation dispersion. *J. Am. Chem. Soc.* **128**, 5262–5269. (doi:10.1021/ja0601540)
 58. Bezsonova I *et al.* 2006 Hydration and packing along the folding pathway of SH3 domains by pressure-dependent NMR. *Biochemistry* **45**, 4711–4719. (doi:10.1021/bi060177r)
 59. Akasaka K, Kitahara R, Kamatari YO. 2013 Exploring the folding energy landscape with pressure. *Arch. Biochem. Biophys.* **531**, 110–115. (doi:10.1016/j.abb.2012.11.016)
 60. Roche J, Royer CA, Roumestand C. 2017 Monitoring protein folding through high pressure NMR spectroscopy. *Prog. Nucl. Magn. Reson. Spectrosc.* **102–103**, 15–31. (doi:10.1016/j.pnmrs.2017.05.003)
 61. Erlach MB, Munte CE, Kremer W, Hartl R, Rochelt D, Niesner D, Kalbitzer HR. 2010 Ceramic cells for high pressure NMR spectroscopy of proteins. *J. Magn. Reson.* **204**, 196–199. (doi:10.1016/j.jmrm.2010.02.011)
 62. Peterson RW, Wand AJ. 2005 Self-contained high-pressure cell, apparatus, and procedure for the preparation of encapsulated proteins dissolved in low viscosity fluids for nuclear magnetic resonance spectroscopy. *Rev. Sci. Instrum.* **76**, 94101. (doi:10.1063/1.2038087)

63. Peterson RW, Nucci NV, Wand AJ. 2011 Modification of encapsulation pressure of reverse micelles in liquid ethane. *J. Magn. Reson.* **212**, 229–233. (doi:10.1016/j.jmr.2011.06.010)
64. Roche J *et al.* 2013 Effect of internal cavities on folding rates and routes revealed by real-time pressure-jump NMR spectroscopy. *J. Am. Chem. Soc.* **135**, 14 610–14 618. (doi:10.1021/ja406682e)
65. Tugarinov V, Libich DS, Meyer V, Roche J, Clore GM. 2015 The energetics of a three-state protein folding system probed by high-pressure relaxation dispersion NMR spectroscopy. *Angew. Chem. Int. Ed.* **54**, 11 157–11 161. (doi:10.1002/anie.201505416)
66. Nguyen LM, Roche J. 2017 High-pressure NMR techniques for the study of protein dynamics, folding and aggregation. *J. Magn. Reson.* **277**, 179–185. (doi:10.1016/j.jmr.2017.01.009)
67. Roche J, Ying J, Maltsev AS, Bax A. 2013 Impact of hydrostatic pressure on an intrinsically disordered protein: a high-pressure NMR study of α -synuclein. *Chembiochem* **14**, 1754–1761. (doi:10.1002/cbic.201300244)
68. McCoy J, Hubbell WL. 2011 High-pressure EPR reveals conformational equilibria and volumetric properties of spin-labeled proteins. *Proc. Natl Acad. Sci. USA* **108**, 1331–1336. (doi:10.1073/pnas.1017877108)
69. Myers JK, Pace CN, Scholtz JM. 1995 Denaturant m values and heat capacity changes: relation to changes in accessible surface areas of protein unfolding. *Protein Sci.* **4**, 2138–2148. (doi:10.1002/pro.5560041020)
70. Meeker AK, García-Moreno B, Shortle D. 1996 Contributions of the ionizable amino acids to the stability of staphylococcal nuclease. *Biochemistry* **35**, 6443–6449. (doi:10.1021/bi960171+)
71. Shortle D. 1989 Probing the determinants of protein folding and stability with amino acid substitutions. *J. Biol. Chem.* **264**, 5315–5318.
72. Karp DA, Gittis AG, Stahley MR, Fitch CA, Stites WE, García-Moreno EB. 2007 High apparent dielectric constant inside a protein reflects structural reorganization coupled to the ionization of an internal Asp. *Biophys. J.* **92**, 2041–2053. (doi:10.1529/biophysj.106.090266)
73. Isom DG, Cannon BR, Castañeda CA, Robinson A, García-Moreno B. 2008 High tolerance for ionizable residues in the hydrophobic interior of proteins. *Proc. Natl Acad. Sci. USA* **105**, 17 784–17 788. (doi:10.1073/pnas.0805113105)
74. Whitten ST, García-Moreno E B. 2000 pH dependence of stability of staphylococcal nuclease: evidence of substantial electrostatic interactions in the denatured state. *Biochemistry* **39**, 14 292–14 304. (doi:10.1021/bi001015c)
75. Wang J, Trucks DM, Abildgaard F, Dzakula Z, Zolnai Z, Markley JL. 1997 Solution structures of staphylococcal nuclease from multidimensional, multinuclear NMR: nuclease-H124 L and its ternary complex with Ca^{2+} and thymidine-3',5'-bisphosphate. *J. Biomol. NMR* **10**, 143–164. (doi:10.1023/A:1018350004729)
76. Loll P, Lattman E. 1989 The crystal structure of the ternary complexes of staphylococcal nuclease Ca^{2+} and the inhibitor PDTP refined at 1.65 Å. *Proteins Struct. Funct. Genet.* **5**, 183–201. (doi:10.1002/prot.340050302)
77. Cotton FA, Hazen, Edward EJ, Legg MJ. 1979 Staphylococcal nuclease: proposed mechanism of action based on structure of enzyme–thymidine 3',5'-bisphosphate–calcium ion complex at 1.5-Å resolution. *Proc. Natl Acad. Sci. USA* **76**, 2551–2555. (doi:10.1073/pnas.76.6.2551)
78. Ho BK, Gruswitz F. 2008 HOLLOW: generating accurate representations of channel and interior surfaces in molecular structures. *BMC Struct. Biol.* **6**, 1–6. (doi:10.1186/1472-6807-8-49)
79. Zweifel ME, Leahy DJ, Hughson FM, Barrick D. 2003 Structure and stability of the ankyrin domain of the *Drosophila* Notch receptor. *Protein Sci.* **12**, 2622–2632. (doi:10.1110/ps.03279003)
80. Huyton T, Wolberger C. 2007 The crystal structure of the tumor suppressor protein pp32 (Anp32a): structural insights into Anp32 family of proteins. *Protein Sci.* **32**, 1308–1315. (doi:10.1110/ps.072803507)
81. Schrodinger LLC. 2015 The PyMOL molecular graphics system, version 1.7.4.
82. Aksel T, Majumdar A, Barrick D. 2011 The contribution of entropy, enthalpy, and hydrophobic desolvation to cooperativity in repeat-protein folding. *Structure* **19**, 349–360. (doi:10.1016/j.str.2010.12.018)
83. Aksel T, Barrick D. 2014 Direct observation of parallel folding pathways revealed using a symmetric repeat protein system. *Biophys. J.* **107**, 220–232. (doi:10.1016/j.bpj.2014.04.058)
84. Dao TP, Majumdar A, Barrick D. 2015 Highly polarized C-terminal transition state of the leucine-rich repeat domain of PP32 is governed by local stability. *Proc. Natl Acad. Sci. USA* **112**, E2298–E2306. (doi:10.1073/pnas.1412165112)
85. Dao TP, Majumdar A, Barrick D. 2014 Capping motifs stabilize the leucine-rich repeat protein PP32 and rigidify adjacent repeats. *Protein Sci.* **23**, 801–811. (doi:10.1002/pro.2462)
86. Panick G, Malessa R, Winter R, Rapp G, Frye KJ, Royer CA. 1998 Structural characterization of the pressure-denatured state and unfolding/refolding kinetics of staphylococcal nuclease by synchrotron small-angle X-ray scattering and Fourier-transform infrared spectroscopy. *J. Mol. Biol.* **275**, 309–402.
87. Roche J *et al.* 2012 Remodeling of the folding free energy landscape of staphylococcal nuclease by cavity-creating mutations. *Biochemistry* **51**, 9535–9546. (doi:10.1021/bi301071z)
88. Frye KJ, Royer CA. 1998 Probing the contribution of internal cavities to the volume change of protein unfolding under pressure. *Protein Sci.* **7**, 2217–2222. (doi:10.1002/pro.5560071020)
89. Till MS, Ullmann GM. 2010 McVol—a program for calculating protein volumes and identifying cavities by a Monte Carlo algorithm. *J. Mol. Model.* **16**, 419–429. (doi:10.1007/s00894-009-0541-y)
90. Caro JA. 2015 Structural origins of pressure effects in proteins. PhD thesis, Johns Hopkins University.
91. Shortle D. 1995 Staphylococcal nuclease: a showcase of m -value effects. *Adv. Protein Chem.* **46**, 217–247. (doi:10.1016/S0065-3233(08)60336-8)
92. Frye KJ, Perman CS, Royer CA. 1996 Testing the correlation between ΔA and ΔV of protein unfolding using m value mutants of staphylococcal nuclease. *Biochemistry* **35**, 10 234–10 239. (doi:10.1021/bi960693p)
93. Mello CC, Barrick D. 2004 An experimentally determined protein folding energy landscape. *Proc. Natl Acad. Sci. USA* **101**, 14 102–14 107. (doi:10.1073/pnas.0403386101)
94. Rouget J-B *et al.* 2010 Unique features of the folding landscape of a repeat protein revealed by pressure perturbation. *Biophys. J.* **98**, 2712–2721. (doi:10.1016/j.bpj.2010.02.044)
95. Rouget J-B, Aksel T, Roche J, Saldana J-L, Garcia AE, Barrick D, Royer CA, Jenkins TC. 2011 Size and sequence and the volume change of protein folding. *J. Am. Chem. Soc.* **133**, 6020–6027.
96. Mohana-Borges R, Silva JL, Ruiz-Sanz J, de Prat-Gay G. 1999 Folding of a pressure-denatured model protein. *Proc. Natl Acad. Sci. USA* **96**, 7888–7893. (doi:10.1073/pnas.96.14.7888)
97. Pappenberger G, Saudan C, Becker M, Merbach AE, Kieffhaber T. 2000 Denaturant-induced movement of the transition state of protein folding revealed by high-pressure stopped-flow measurements. *Proc. Natl Acad. Sci. USA* **97**, 17–22. (doi:10.1073/pnas.97.1.17)
98. Kitahara R, Royer C, Yamada H, Boyer M, Saldana J-LJ-LL, Akasaka K, Roumestand C. 2002 Equilibrium and pressure-jump relaxation studies of the conformational transitions of P13(MTCP1). *J. Mol. Biol.* **320**, 609–628. (doi:10.1016/S0022-2836(02)00516-8)
99. Mei G, Di Venere A, Campeggi FM, Gilardi G, Rosato N, De Matteis F, Finazzi-Agrò A. 1999 The effect of pressure and guanidine hydrochloride on azurins mutated in the hydrophobic core. *Eur. J. Biochem.* **265**, 619–626. (doi:10.1046/j.1432-1327.1999.00751.x)
100. Sasahara K, Nitta K. 1999 Pressure-induced unfolding of lysozyme in aqueous guanidinium chloride solution. *Protein Sci.* **8**, 1469–1474. (doi:10.1110/ps.8.7.1469)
101. Brun L *et al.* 2006 Hydration of the folding transition state ensemble of a protein. *Biochemistry* **45**, 3473–3480. (doi:10.1021/bi052638z)
102. Mitra L *et al.* 2007 V(i)-value analysis: a pressure-based method for mapping the folding transition state ensemble of proteins. *J. Am. Chem. Soc.* **129**, 14 108–14 109. (doi:10.1021/ja073576y)
103. Schlessman JL, Abe C, Gittis A, Karp DA, Dolan MA, García-Moreno EB, García-Moreno B. 2008 Crystallographic study of hydration of an internal cavity in engineered proteins with buried polar or ionizable groups. *Biophys. J.* **94**, 3208–3216. (doi:10.1529/biophysj.107.122473)
104. Harms MJ, Castañeda CA, Schlessman JL, Sue GR, Isom DG, Cannon BR, García-Moreno B.

- 2009 The pK_a values of acidic and basic residues buried at the same internal location in a protein are governed by different factors. *J. Mol. Biol.* **389**, 34–47. (doi:10.1016/j.jmb.2009.03.039)
105. Fossat MJ *et al.* 2016 High-resolution mapping of a repeat protein folding free energy landscape. *Biophys. J.* **111**, 2368–2376. (doi:10.1016/j.bpj.2016.08.027)
106. Kitahara R *et al.* 2011 Structural plasticity of staphylococcal nuclease probed by perturbation with pressure and pH. *Proteins* **79**, 1293–1305. (doi:10.1002/prot.22966)
107. Roche J *et al.* 2013 Structural, energetic, and dynamic responses of the native state ensemble of staphylococcal nuclease to cavity-creating mutations. *Proteins* **81**, 1069–1080. (doi:10.1002/prot.24231)
108. Li H, Akasaka K. 2006 Conformational fluctuations of proteins revealed by variable pressure NMR. *BBA-Proteins Proteom.* **1764**, 331–345. (doi:10.1016/j.bbapap.2005.12.014)
109. Noel JK, Whitford PC, Sanbonmatsu KY, Onuchic JN. 2010 SMOG@ctbp: simplified deployment of structure-based models in GROMACS. *Nucleic Acids Res.* **38**, W657–W661. (doi:10.1093/nar/gkq498)
110. Rotkiewicz P, Skolnick J. 2008 Fast procedure for reconstruction of full-atom protein models from reduced representations. *J. Comp. Chem* **29**, 1460–1465. (doi:10.1002/jcc.20906)
111. Bédard S, Mayne LC, Peterson RW, Wand AJ, Englander SW. 2008 The foldon substructure of staphylococcal nuclease. *J. Mol. Biol.* **376**, 1142–1154. (doi:10.1016/j.jmb.2007.12.020)
112. Skinner JJ, Lim WK, Bédard S, Black BE, Englander SW. 2012 Protein dynamics viewed by hydrogen exchange. *Protein Sci.* **21**, 996–1005. (doi:10.1002/pro.2081)
113. Kamagata K, Sawano Y, Tanokura M, Kuwajima K. 2003 Multiple parallel-pathway folding of proline-free staphylococcal nuclease. *J. Mol. Biol.* **332**, 1143–1153. (doi:10.1016/j.jmb.2003.07.002)
114. Maki K, Cheng H, Dolgikh DA, Shastry MCR, Roder H. 2004 Early events during folding of wild-type staphylococcal nuclease and a single-tryptophan variant studied by ultrarapid mixing. *J. Mol. Biol.* **338**, 383–400. (doi:10.1016/j.jmb.2004.02.044)
115. Maki K, Cheng H, Dolgikh DA, Roder H. 2007 Folding kinetics of staphylococcal nuclease studied by tryptophan engineering and rapid mixing methods. *J. Mol. Biol.* **368**, 244–255. (doi:10.1016/j.jmb.2007.02.006)
116. Zhang Y *et al.* 2018 High pressure NMR and SAXS reveals how capping modulates folding cooperativity of the pp32 leucine rich repeat protein. *J. Mol. Biol.* **430**, 1336–1349. (doi:10.1016/j.jmb.2018.03.005)
117. Jenkins KA, Fossat MJ, Zhang S, Rai DK, Klein S, Gillilan R, White Z, Gerlich G, McCallum SA, Winter R, Gruner SM, Barrick D, Royer CA. 2018 The consequences of cavity creation on the folding landscape of a repeat protein depend upon context. *Proc. Natl Acad. Sci. USA* **115**, E8153–E8161.
118. Main ERG, Stott K, Jackson SE, Regan L. 2005 Local and long-range stability in tandemly arrayed tetratricopeptide repeats. *Proc. Natl Acad. Sci. USA* **102**, 5721–5726. (doi:10.1073/pnas.0404530102)
119. D'Andrea LD, Regan L. 2003 TPR proteins: the versatile helix. *Trends Biochem. Sci.* **28**, 655–662. (doi:10.1016/j.tibs.2003.10.007)
120. Bella J, Hindle KL, McEwan PA, Lovell SC. 2008 The leucine-rich repeat structure. *Cell. Mol. Life Sci.* **65**, 2307–2333. (doi:10.1007/s00018-008-8019-0)
121. Babu CR, Hilser VJ, Wand AJ. 2004 Direct access to the cooperative substructure of proteins and the protein ensemble via cold denaturation. *Nat. Struct. Mol. Biol.* **11**, 352–357. (doi:10.1038/nsmb739)
122. Vidugiris GJA, Markley JL, Royer CA. 1995 Evidence for a molten globule-like transition state in protein folding from determination of activation volumes. *Biochemistry* **34**, 4909–4912.
123. Woenckhaus J, Köhling R, Thiyagarajan P, Littrell KC, Seifert S, Royer CA, Winter R. 2001 Pressure-jump small-angle X-ray scattering detected kinetics of staphylococcal nuclease folding. *Biophys. J.* **80**, 1518–1523. (doi:10.1016/S0006-3495(01)76124-3)
124. Walkenhorst WF, Green SM, Roder H. 1997 Kinetic evidence for folding and unfolding intermediates in staphylococcal nuclease. *Biochemistry* **36**, 5795–5805. (doi:10.1021/bi9700476)